New biomass derived carbon catalysts for biomass valorization

Lakhya Jyoti Konwar

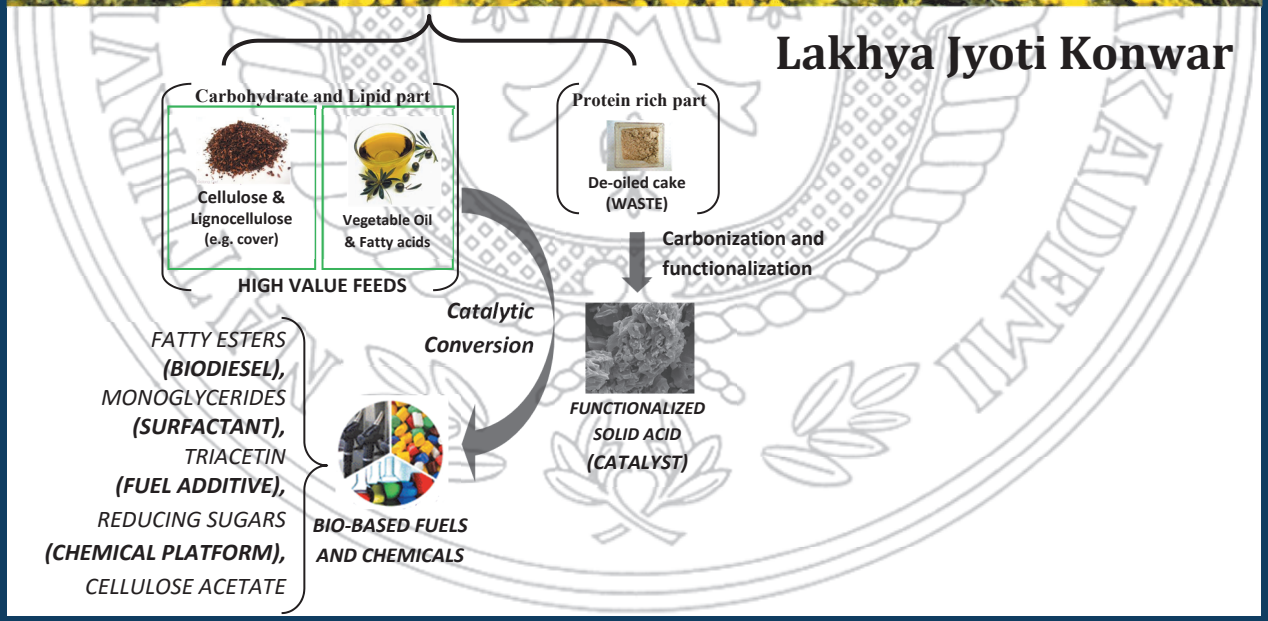

Johan Gadolin Process Chemistry Centre
Laboratory of Industrial Chemistry and Reaction engineering
Faculty of Science and Engineering
Åbo Akademi University
Turku/Åbo, 2016

New biomass derived carbon catalysts for biomass valorization

Doctoral thesis

Lakhya Jyoti Konwar

Johan Gadolin
Process Chemistry Centre

Laboratory of Industrial Chemistry and Reaction Engineering
Faculty of Science and Engineering
Åbo Akademi University
Turku/Åbo, 2016

Supervised by

Professor Jyri-Pekka Mikkola
Åbo Akademi University, Finland & Umeå University, Sweden

Docent Dr. Päivi Mäki-Arvela
Åbo Akademi University, Finland

Reviewers

Docent Dr. Ahmad Kalantar Neyestanaki, Shell Global Solutions International BV, Amsterdam (ahmad.kalantar@shell.com)

and

Prof. Docent Dr. Ákos Kukovecz, University of Szeged, Faculty of Science and Informatics, Department of Applied and Environmental Chemistry, group head of the MTA-SZTE "Lendület" Porous Nanocomposites Research Group (kakos@chem.u-szeged.hu)

Opponent

Docent Dr. Ahmad Kalantar Neyestanaki, Shell Global Solutions International BV, Amsterdam (ahmad.kalantar@shell.com)

ISBN 978-952-12-3395-1 (print)
ISBN 978-952-12-3396-8 (PDF)
Painosalama Oy – Turku, Finland 2016

Preface

The present work has been carried out at the Laboratory of Industrial Chemistry and Reaction Engineering, Johan Gadolin Process Chemistry Centre, Åbo Akademi University (Turku, Finland) and Tezpur University (Tezpur, India). The research is part of the activities at Åbo Akademi Johan Gadolin Process Chemistry Centre, a centre of excellence financed by Åbo Akademi University.

The financial support from the Center for International Mobility in the form of CIMO fellowship is gratefully acknowledged. I am also thankful to the Department of Science and Technology, India and the Academy of Finland for the initiation of the research programme between India and Finland and funding the numerous research visits between Åbo Akademi University and Tezpur University.

At the very outset I would like to express my most sincere gratitude to my advisors Professor Jyri-Pekka Mikkola and Docent Päivi Mäki-Arvela for giving me the opportunity to work at the Laboratory of Industrial Chemistry and Reaction Engineering, Åbo Akademi University. I remain grateful to Professor Mikkola and Dr. Mäki-Arvela for all they have done for me and keep on doing within science and much beyond. I would like to thank Docent Narendra Kumar for sharing his wealth of experience in zeolites and catalyst characterization techniques. I am also grateful to Docent Johan Wärnå for his invaluable help and suggestions in kinetic modeling. I am also thankful to the supervisors of my Indian thesis, Professor Ashim Jyoti Takur and Professor Dhanapati Deka at Tezpur University, for allowing me to use their laboratory facilities to perform some of the experimental works related to the thesis. I am also thankful to Dr. Anil K. Sarma (Sci. E, SSS-NIRE, MNRE, India) for his suggestions and advice on science and beyond.

Further, I would also like to take the opportunity to acknowledge the help and suggestions received from all of my co-authors who have contributed to my thesis; in particular, Professor Ramesh Ch. Deka and his Theoretical Chemistry Group (Pakiza Begum) at Tezpur University (India) are gratefully acknowledged for molecular modeling of reaction products and intermediates. I am also thankful to Laboratory Manager, Dr. Kari Eränen for his invaluable help and tips with the reactors and analytical systems.

I would like to express my gratitude to all the members of the Laboratory of Industrial Chemistry and Reaction Engineering, Åbo Akademi University for cooperation, especially Dr. Eero Salminen, Dr. Toni Riittonen, Dr. Bartosz Rozmyslowicz, Dr. Jussi Rissanen for valuable assistance and help as well as to everybody who has made my visits/stay at the Laboratory memorable.

Finally, I would like to take the opportunity to thank my family (Maa, Deuta, Kaku) and friends (Prasanta, Pankaj, Arup) for their love and support throughout the years. I remain ever thankful to my mother and to my wife Rupali for their patience, understanding and unconditional love.

Lakhya Jyoti Konwar, Åbo, February 2016

Abstract

New biomass derived carbon catalysts for biomass valorization

Lakhya Jyoti Konwar

Doctoral Thesis, Laboratory of Industrial Chemistry and Reaction Engineering, Johan Gadolin Process Chemistry Centre, Faculty of Science and Engineering, Åbo Akademi University, 2016.

Due to diminishing petroleum reserves, unsteady market situation and the environmental concerns associated with utilization of fossil resources, the utilization of renewables for production of energy and chemicals (biorefining) has gained considerable attention. Biomass is the only sustainable source of organic compounds that has been proposed as petroleum equivalent for the production of fuels, chemicals and materials. In fact, it would not be wrong to say that the only viable answer to sustainably convene our future energy and material requirements remain with a *bio-based economy* with biomass based industries and products. This has prompted biomass valorization (biorefining) to become an important area of industrial research. While many disciplines of science are involved in the realization of this effort, catalysis and knowledge of chemical technology are considered to be particularly important to eventually render this dream to come true.

Traditionally, the catalyst research for biomass conversion has been focused primarily on commercially available catalysts like zeolites, silica and various metals (Pt, Pd, Au, Ni) supported on zeolites, silica etc. Nevertheless, the main drawbacks of these catalysts are coupled with high material cost, low activity, limited reusability etc. – all facts that render them less attractive in industrial scale applications (poor activity for the price). Thus, there is a particular need to develop active, robust and cost efficient catalytic systems capable of converting complex biomass molecules.

Saccharification, esterification, transesterification and acetylation are important chemical processes in the valorization chain of biomasses (and several biomass components) for production of platform chemicals, transportation fuels, food additives and materials. In the current work, various novel acidic carbons were synthesized from wastes generated from biodiesel and allied

industries, and employed as catalysts in the aforementioned reactions. The structure and surface properties of the novel materials were investigated by XRD, XPS, elemental analysis, SEM, TEM, TPD and N_2-physisorption techniques.

The agro-industrial waste derived sulfonic acid functionalized novel carbons exhibit excellent catalytic activity in the aforementioned reactions and easily outperformed liquid H_2SO_4 and conventional solid acids (zeolites, ion-exchange resins etc). The experimental results indicated strong influence of catalyst pore-structure (pore size, pore-volume), concentration of $–SO_3H$ groups and surface properties in terms of the activity and selectivity of these catalysts. Here, a large pore catalyst with high $–SO_3H$ density exhibited the highest esterification and transesterification activity, and was successfully employed in biodiesel production from fatty acids and low grade acidic oils. Also, a catalyst decay model was proposed upon biodiesel production and could explain that the catalyst loses its activity mainly due to active site blocking by adsorption of impurities and by-products.

The large pore sulfonated catalyst also exhibited good catalytic performance in the selective synthesis of triacetin via acetylation of glycerol with acetic anhydride and out-performed the best zeolite H-Y with respect to reusability. It also demonstrated equally good activity in acetylation of cellulose to soluble cellulose acetates, with the possibility to control cellulose acetate yield and quality (degree of substitution, DS) by a simple adjustment of reaction time and acetic anhydride concentration.

In contrast, the small pore and highly functionalized catalysts obtained by hydrothermal method and from protein rich waste (Jatropha de-oiled waste cake, DOWC), were active and selective in the esterification of glycerol with fatty acids to monoglycerides and saccharification of cellulosic materials, respectively. The operational stability and reusability of the catalyst was found to depend on the stability of $–SO_3H$ function (leaching) as well as active site blocking due to adsorption of impurities during the reaction. Thus, our results corroborate the potential of DOWC derived sulfated mesoporous active carbons as efficient integrated solid acid catalysts for valorization of biomass to platform chemicals, biofuel, bio-additive, surfactants and cellulose-esters.

Referat

Nya biomassabaserade kolkatalysatorer för omvandling av biomassa

Lakhya Jyoti Konwar

Doktorsavhandling, Laboratoriet for teknisk kemi och reaktionsteknik, Johan Gadolin Processkemiska Centret, Fakulteten för naturvetenskaper och teknik, Åbo Akademi, 2016.

Tack vare sinande tillgångar av fossila råmaterial, fluktuerande marknad samt miljöproblem associerade till utnyttjandet av fossila råmaterial har utnyttjandet av förnybara råmaterial för framställning av energi och kemikalier (bioraffinering) fått mycket uppmärksamhet. Biomassan är en hållbar källa för organiska komponenter som tävlar med fossila råmaterial vid framställning av bränslen, kemikalier och material. Det är inte felaktigt att säga att den ända möjligheten med tanke på framtidens hållbara utveckling är att utveckla biomassa-utnyttjande ekonomi som baseras påbiomassabaserad industri och produkter. Allt detta har lett till att utnyttjande av förnybara råmaterial (bioraffinaderi) har blivit ett mycket viktigt forskningsområde för industrin. Även ommånga olika vetenskapsgrenar behövs för att förverkliga denna dröm, är katalys och kunskaper i kemisk teknologi mycket viktiga i detta sammanhang.

Traditionellt har biomassa omvandlingen haft fokus i att använda primärt kommersiella katalysatorer, dvs zeoliter, kiseldioxid och metaller på bärarmaterial (Pt, Pd, Au, Ni). De största nackdelarna med dessa katalysatorer är materialens höga priser, låg aktivitet, begränsad återanvändbarhet osv.varvid det är mindre attraktivtattanvändadenna typ av katalysatorer i industriell skala (låg aktivitet samt högt pris). Därmed är det motiveratatt utveckla nya aktiva, hållbara och billiga katalytiska material som möjliggör omvandling av komplexa biomassamolekyler.

Sackkarifiering, förestring, transförestring och acetylering är all viktiga kemiska processer vid konvertering av olika biomassabaserade molekyler till kemikalier, drivmedel, tillsatsämnen till mat och material. I detta arbete har olika nya sura kolmaterial syntetiserats ur avfall som härstammarfrån biodieselframställning och relaterade industrier. Dessa material har vidare använts som katalysatoreri de ovannämnda reaktionerna. Strukturen och ytegenskaperna hosde nya

materialen har undersökts med diverse tekniker såsom XRD, XPS, elementär analys, SEM, TEM, TPD och kväve fysisorption.

Nya kolmaterial funktionaliserade med sulfonsyra och framställda ur avfall från jordbruk och industrivisade sig ha utmärktakatalytiskaegenskaperi de ovannämnda reaktioner och den katalytiskaaktiviteten varhögreän vad som kanuppnås med hjälp av svavelsyra och konventionella fasta surakatalysatorer (zeoliter, jonbyteshartser osv). De experimentella resultaten visade att katalysatorns porstruktur (porstorlek, porvolym), koncentration av–SO_3H grupper och ytegenskaperkorrelerade med katalysatorernasaktivitet och selektivitet. Katalysatorer med stora porer och en hög –SO_3H täthet hade den bästa prestandan iförestrings- och transförestring och användes framgångsrikt vid framställning av biodiesel från fettsyror och sura oljor av låg kvalitet. Vidare, även katalysatornsdeaktiveringsmodel utvecklades för biodiesel framställning och modellen kunde förklara den avtagande reaktions hastigheten huvudsakligen förorsakat av tilltäppning av de aktiva säten på katalysatoryta genom adsorption av föroreningar.

Den sulfonerade katalysatorn med stora porer var också katalytiskt aktiv i selektiv syntes av triacetin genom acetylering av glycerol med ättiksyra anhydrid och den hade ytterligare en prestationsförmåga jämfört med den för H-Y zeolit i avseende å återanvändning. Denna katalysator var också aktiv i acetylering av cellulosa till lösliga cellulosaacetater och möjliggjorde kontroll av substitueringsgraden hos cellulosaacetat genom en enkel justeringav reaktionstiden och mängden av ättiksyraanhydrid.

I motsats, katalysatorer med små porer och framställa via en hydrotermisk metod ur proteinhaltigt avfall (Jatropha de oljade avfall tårta, DOWC) var aktiva vid selektiv förestring av glycerol med fettsyror till monosackarider och sackarifiering av cellulosa. Stabilitetoch återanvändning av katalysatorn påvisades varaberoende av stabilitetenhos –SO_3H grupper (upplösning) samt av tilltäppning av aktiva säten genom adsorption av föroreningar under reaktionens förlopp. Dessa resultat visar tydligt potentialen hossulfonerade DOWC baserade mesoporösa, aktiva kolkatalysatorer vid omvandling av biomassa till kemikalier, biobränsle, biotillsatsämnen, ytaktiva ämnen och cellulosaestrar.

বিমূর্ত

জৈববস্তুপুঞ্জ উচ্চমূল্য জন্য নতুন জৈববস্তুপুঞ্জ প্রাপ্ত কার্বন অনুঘটক

লক্ষ্য জ্যোতি কোঁৱর

ডক্টরেট থিসিস, রসায়ন শিল্প ও প্রতিক্রিয়া প্রকৌশল এর ল্যাবরেটরি, Johan Gadolin প্রক্রিয়া রসায়ন সেন্টার, বিজ্ঞান ও প্রকৌশল অনুষদের, Åbo আকাদেমি বিশ্ববিদ্যালয়, 2016।

দরুন জীবাশ্ম সম্পদের সদ্ব্যবহার যুক্ত কমা পেট্রোলিয়াম মজুদ, নড়বড় বাজার পরিস্থিতি ও পরিবেশ উদ্বেগের, জ্বালানি ও কেমিক্যাল (biorefining) উৎপাদনের জন্য নবায়নযোগ্য ব্যবহার যথেষ্ট মনোযোগ অর্জন করেছে। জৈববস্তুপুঞ্জ জ্বালানির, কেমিক্যাল ও পদার্থ উৎপাদন পেট্রোলিয়াম সমতুল্য হিসেবে প্রস্তাব করা হয়েছে যে জৈব যৌগের শুধুমাত্র টেকসই উৎস। বস্তুত, এটা একমাত্র টেকসই উত্তর পরিবেশবান্ধব আমাদের ভবিষ্যত শক্তি ও বস্তুগত প্রয়োজনীয়তা জৈববস্তুপুঞ্জ ভিত্তিক শিল্প ও পণ্যের সঙ্গে একটি বায়ো-ভিত্তিক অর্থনীতির সঙ্গে থাকা আহ্বান করা বলে ভুল হবে না। এই অনুরোধ জানানো হয়েছে জৈববস্তুপুঞ্জ উচ্চমূল্য (biorefining) শিল্প গবেষণা একটি গুরুত্বপূর্ণ এলাকা পরিণত। বিজ্ঞানের অনেক নিয়মানুবর্তিতা এই প্রচেষ্টা, অনুঘটন আদায় জড়িত হয় ও রাসায়নিক প্রযুক্তি জ্ঞান বিশেষভাবে গুরুত্বপূর্ণ বলে মনে করা হয় যদিও শেষ পর্যন্ত খাটা এই স্বপ্ন রেন্ডার।

প্রথাগতভাবে, জৈববস্তুপুঞ্জ রূপান্তর জন্য ক্যাটালিস্ট গবেষণা যাইহোক, এই অনুঘটক প্রধান অপূর্ণতা সঙ্গে মিলিত হয় zeolites, সিলিকা এবং zeolites সমর্থিত বিভিন্ন ধাতু (Pt, Pd, Au, Ni), সিলিকা ইত্যাদি বাণিজ্যিকভাবে উপলব্ধ অনুঘটক প্রাথমিকভাবে দৃষ্টি নিবদ্ধ করা হয়েছে উচ্চ উপাদান খরচ, কম কার্যকলাপ সীমিত পুনর্ব্যাবহার্যোগ্যতা ইত্যাদি-সব (মূল্য জন্য দরিদ্র কার্যকলাপ) শিল্প স্কেল অ্যাপ্লিকেশনের মধ্যে তাদের কম আকর্ষণীয় রেন্ডার যে তথ্য। সুতরাং, জটিল জৈববস্তুপুঞ্জ অণু রূপান্তর করতে সক্ষম, সক্রিয় শক্তসমর্থ এবং খরচ কার্যকর অনুঘটকের সিস্টেম বিকাশ একটি নির্দিষ্ট প্রয়োজন নেই।

Saccharification, esterification, transesterification এবং acetylation প্ল্যাটফর্ম কেমিক্যাল, পরিবহন জ্বালানী খাদ্য additives এবং উপকরণ উৎপাদনের জন্য জৈববস্তুপুঞ্জ (এবং বিভিন্ন জৈববস্তু উপাদান) এর উচ্চমূল্য শৃঙ্খল গুরুত্বপূর্ণ রাসায়নিক প্রক্রিয়া হয়। বর্তমান কাজের মধ্যে, বিভিন্ন উপন্যাস আল্গিক কার্বন বায়োডিজেল এবং সংশ্লিষ্ট শিল্পের থেকে উত্পন্ন বর্জ্য থেকে সংশ্লেষিত হয় এবং উপরোক্ত প্রতিক্রিয়া মধ্যে অনুঘটক হিসেবে নিযুক্ত। উপন্যাস উপকরণ গঠন এবং পৃষ্ঠ বৈশিষ্ট্য XRD, XPS, আধিভৌতিক বিশ্লেষণ, SEM, TEM, TPD এবং N_2-physisorption কৌশল দ্বারা তদন্ত করা হয়েছিল।

sulfonic অ্যাসিড প্রাপ্ত কৃষি শিল্প বর্জ্য উপন্যাস কার্বন উপরোক্ত প্রতিক্রিয়া চমৎকার অনুঘটকের কার্যকলাপ এবং সহজেই ছাপিয়ে তরল H_2SO_4 এবং প্রচলিত কঠিন অ্যাসিড (zeolites, আয়ন-বিনিময় রজন ইত্যাদি) প্রদর্শিত ক্রিয়াশীল। পরীক্ষামূলক ফলাফল এই অনুঘটক কার্যকলাপ এবং নির্বাচনশীলতা পরিপ্রেক্ষিতে ক্যাটালিস্ট দড়ি কাঠামো (বিল আকার, দড়ি ভলিউম), $-SO_3H$ গ্রুপ এবং পৃষ্ঠ বৈশিষ্ট্য ঘনত্ব শক্তিশালী প্রভাব নির্দেশিত। এখানে, উচ্চ $-SO_3H$ ঘনত্ব সঙ্গে একটি বৃহৎ বিল অনুঘটক সর্বোচ্চ esterification এবং transesterification কার্যকলাপ বিকশিত এবং সফলভাবে ফ্যাটি এবং কম গ্রেড আল্গিক তেল থেকে বায়োডিজেল উৎপাদন নিযুক্তি ছিল। এছাড়াও, একটি অনুঘটক ক্ষয় মডেল বায়োডিজেল

উৎপাদন উপর প্রস্তাব করেন এবং অনুঘটক কারণে অমেধ্য পরিশোষণ করে সক্রিয় সাইটে ব্লক এবং উপজাত প্রধানত তার কার্যকলাপ হারায় যে ব্যাখ্যা করতে পারে।

বড় লোমকূপ sulfonated ক্যাটালিস্ট এছাড়াও অ্যাসিটিক anhydride সঙ্গে এবং আউট-সঞ্চালিত পুনর্ব্যাবহার্যোগ্যতা সম্মান সঙ্গে সেরা জেওলীট্ H-Y গ্লিসারিন নিয়ে acetylation মাধ্যমে triacetin নির্বাচনী সংশ্লেষণ ভাল অনুঘটকের কর্মক্ষমতা বিকশিত। এটি প্রতিক্রিয়া সময় এবং অ্যাসিটিক anhydride ঘনত্ব সহজ সমন্বয় দ্বারা সেলুলোজ সির্কাল্পদ্বারা জারিত ফলন ও গুণগত মান (অনুকল্প ডিগ্রী, DS নিয়ন্ত্রণ করার সম্ভাবনা সঙ্গে, দ্রবণীয় সেলুলোজ acetates করতে সেলুলোজ acetylation সমানভাবে ভাল কার্যকলাপ প্রদর্শন।

বিপরীতভাবে, ছোট pore এবং জলবিদ্যুত পদ্ধতি দ্বারা এবং প্রোটিন সমৃদ্ধ বর্জ্য থেকে প্রাপ্ত অত্যন্ত ক্রিয়াশীল অনুঘটক (জাত্রোফা ডি-চুর বর্জ্য পিষ্টক, DOWC), ফ্যাটি সঙ্গে সক্রিয় ও গ্লিসারিন নিয়ে esterification নির্বাচনী ছিল cellulosic উপকরণ monoglycerides এবং saccharification করতে, যথাক্রমে। ক্যাটালিস্ট কর্মক্ষম স্থায়িত্ব এবং পুনর্ব্যাবহার্যোগ্যতা -SO_3H ফাংশন (ক্ষরণ) সেইসাথে প্রতিক্রিয়া সময় অমেধ্য পরিশোষণ কারণে ব্লক সক্রিয় সাইটের স্থিতিশীলতার উপর নির্ভর করতে পাওয়া যায় নি. সুতরাং, আমাদের ফলাফল DOWC সম্ভাবনাময় প্ল্যাটফর্ম কেমিক্যাল, জৈব জ্বালানি, বায়ো-যুত, surfactants এবং সেলুলোজ-এস্টার যাও জৈববস্তু উচ্চমূল্য জন্য দক্ষ সমন্বিত কঠিন এসিড অনুঘটক হিসেবে mesoporous সক্রিয় কার্বন sulfated প্রাপ্ত সুনিশ্চিত।

List of publications and related presentations

[I]. **Lakhya Jyoti Konwar,** Päivi Mäki-Arvela, Eero Salminen, Narendra Kumar, Ashim Jyoti Thakur, Jyri-Pekka Mikkola, Dhanapati Deka. Towards carbon efficient biorefining: Multifunctional mesoporous solid acids obtained from biodiesel production wastes for biomass conversion. Appl. Cat. B Env., 176–177, 20–35, 2015.

[II]. **Lakhya Jyoti Konwar**, Johan Wärnå, Päivi Mäki-Arvela, Narendra Kumar, Jyri-Pekka Mikkola. Reaction kinetics with catalyst deactivation in simultaneous esterification and transesterification of acid oils to biodiesel (FAME) over a mesoporous sulphonated carbon catalyst, Fuel, 166, 1-11, 2016**.**

[III]. **Lakhya Jyoti Konwar,** Päivi Mäki-Arvela, Pakiza Begum, Narendra Kumar, Ashim Jyoti Thakur, Jyri-Pekka Mikkola, Ramesh Chandra Deka, Dhanapati Deka. Shape selectivity and acidity effects in glycerol acetylation with acetic anhydride: Selective synthesis of triacetin over Y-Zeolite and sulfonated mesoporous carbons, J. Catal., 329, 237-247, 2015.

[IV]. **Lakhya Jyoti Konwar**, Päivi Mäki-Arvela, Narendra Kumar, Jyri-Pekka Mikkola, Anil Kumar Sarma, Dhanapati Deka. Selective esterification of fatty acids with glycerol to monoglycerides over $–SO_3H$ functionalized carbon catalysts, React.Kin.Mech.Cat. 2016 (accepted, in press)

[V]. **Lakhya Jyoti Konwar**, Päivi Mäki-Arvela, Ashim Jyoti Thakur, Narendra Kumar, Jyri-Pekka Mikkola. Sulfonated carbon as a new, reusable heterogeneous catalyst for one-pot synthesis of acetone soluble cellulose acetate, RSC Advances, 6, 8829-8837, 2016.

[VI]. **Lakhya Jyoti Konwar**, Yasuhito Sugano, Rahul Singh Chutia, Päivi Mäki-Arvela, Rupam Kataki, Jyri-Pekka Mikkola. Sustainable synthesis of N and P co-doped porous amorphous carbon using oil seed processing wastes, Materials letters, 173, 145–148, 2016.

[VII]. **Lakhya Jyoti Konwar**, Ashim Jyoti Thakur, Päivi Mäki-Arvela, Narendra Kumar, Jyri-Pekka Mikkola, Dhanapati. Deka, Preparation of surface modified mesoporous carbons from agro-industrial waste for catalytic applications (India / Finland / SwedenP106), The 11^{th} International Symposium on the Scientific Bases for the Preparation of Heterogeneous Catalysts. July 6-10, 2014, Louvain-la-Neuve, Belgium. (Poster presentation)

Author's contribution to articles I-V

Lakhya Jyoti Konwar carried out the experiments and wrote the articles. Help in kinetic modelling was provided by J.-P. Mikkola and Johan Wärnå

Contents

1. Introduction

1.1. Biomass and biorefinery concept

The use of renewables for production of energy and chemicals (biorefining) has gained considerable importance in recent years due to the diminishing petroleum reserves, its unstable market fluctuations and partly due to the environmental concerns associated with its exploration and use. Biomass is an ideal alternative to fossil resources and the only sustainable source of organic compounds which has been proposed as petroleum equivalent for the production of fuels, chemicals and materials. In other words, the only viable answer to sustainably convene our future energy and material requirements remains with a *bio-based economy* with biomass-based industries and products. Thus, development of new, efficient technologies for producing energy and materials from sustainable resources has prompted biomass valorization (biorefining) to become an important area of industrial research, and is presently considered as a key step towards the realization of sustainable future industries.[1,2] However, compared to petroleum, the cost of processing biomass/renewables into useful products (fuels and chemicals) is still too high, making these products less competitive in the current market. Nonetheless, the same may not be true when the petroleum (crude oil) price goes up in the future. The difficulty with regard to the conversion of biomass and biomass components is mainly due to its complex chemical nature which is very different from crude oil, making it a very difficult feed to be converted/processed using existing refining technologies. Further, the currently available biomass conversion technologies (bio-chemical, thermochemical and catalytic) employ expensive enzymes, homogeneous catalysts, such as HCl, H_2SO_4, NaOH, KOH, and specialized equipment leading to significantly increased upstream, as well as downstream processing costs (as purification, separation and waste generation become unavoidable) which also create a major bottleneck for their large scale commercialization.[3,4] In terms of chemical composition, petroleum (crude/fossil oil) is essentially a mixture of various hydrocarbons and organic compounds of different molecular weights, it can be fractionated and converted into useful products by simple distillation. Biomass, on the other hand, has a more complex polymeric structure and is composed of highly functionalized oxygenated molecules, such as glucose, amino acids and aromatics as building units; main components of biomass (ash free basis) are carbohydrates (starch, cellulose, and hemicellulose), lipids (fatty acids, fatty glycerides, extractive oils), lignin (phenolics,

absent in some verities, e.g. algae) and proteins (Figure 1.1). Consequently, the conversion of biomass is more challenging. However, biomass has advantages in terms of long-term sustainability, low sulfur content etc. Thus, efficient valorization of such renewable feeds require many innovations in the entire process chain ranging from crop yield optimization by bioengineering, improved pretreatment processes to break up biomass feed into its components and finally selective, energy and resource-efficient conversion of the constituents into useful products (value-added fuels, chemicals and materials).[3-5]

Generally, biomass rich in carbohydrates (wood, pulp etc.) is considered as a good feedstock for conversion via hydrolytic pathways into platform molecules (5-hydroxymethylfurfural, sugars, furfural, etc.) and bio-alcohols while lipid rich biomass (oil seed, oleaginous plant, algae) are more suitable for conversion into biodiesel (via transesterification) and hydrocarbon fuels like green diesel (via hydrocracking that can also produce gasoline and propane as by-products).[5,6]

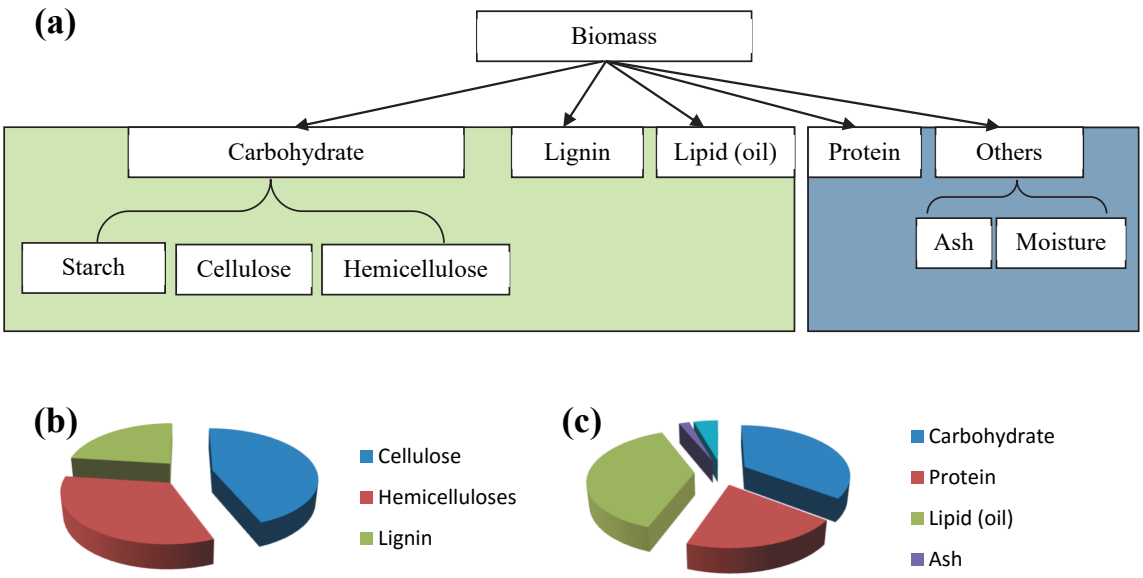

Figure 1.1. (a) Components of biomass, (b) typical composition of woody (lignocellulosic) biomass (ash free basis) and (c) typical composition of oligogenous biomass (oil seeds).

1.2. Catalytic conversion of biomass

While many disciplines of science and engineering are involved in the effort to develop technologies for production of fuels, chemicals and materials from biomass resources, one field in particular is considered to be instrumental to the eventual realization of these biomass-based refineries: catalysis. Also, among the currently available conversion technologies, catalytic (thermochemical and hydrolytic) routes are industrially more attractive as they offer the fastest conversion rate with wider product range and controllable selectivity for conversion of biomass (or biomass-platform molecules) into useful products (functional chemicals, additives and liquid fuels). A schematic summary of the different catalytic strategies to convert the biomass components into fuels and chemicals is shown in Figure 1.2.[6]

Currently, the two main catalytic pathways to transform biomass and biomass platform molecules into useful fuels and chemicals are thermochemical (gasification, pyrolysis) and hydrolytic conversion. While gasification and pyrolysis processes deal with the whole biomass leading to upgradeable platforms, such as synthesis gas, bio-oil and biochar, hydrolysis on the other hand is a more complicated process which requires the polymeric units of biomass to be broken into its constituent monomeric units (sugars, amino acids, fatty acids) for subsequent conversion into platform molecules and useful products using chemical reactions (Figure 1.2). Even though hydrolysis-based platforms are associated with higher upstream costs arising from the complicated pretreatment and hydrolysis steps, the advantage here is that the aqueous solutions of biomass-derived compounds could be processed selectively to yield a variety of organic compounds (including hydrocarbons) with targeted molecular weights and structures which renders this technology more attractive from a biorefinery prospective. As an example, sugars (a hydrolysis platform of biomass) can be used as reforming feeds for the production of renewable H_2, or they can be dehydrated to yield furfurals or levulinic acid. For each of these platforms, researchers have already suggested relevant strategies for the formation of C–C bonds, such as aldol condensation of ketones and oligomerization of alkenes, to enable the production of useful hydrocarbon products like gasoline, jet, and diesel fuel. Research conducted in industry and academia has investigated the aforementioned reaction strategies (in particular hydrolysis, hydrogenation, esterification, transesterification, condensation, dehydration, etherification, C-C coupling, aqueous phase reforming (APR) and hydrolytic hydrogenation) with different catalysts

(zeolites, ion exchange resins, mesoporous silica, metal oxides, mixed oxides, metal supported catalysts etc.) to achieve desired conversion and selectivity for upgrading biomass into useful products (fuels and chemicals).[5-7] In addition to this, many biomass derivatives (cellulose, fatty acids, levulinic acid, glycerol etc) contain highly reactive functionalities/functional groups like –OH, –COOH which make them suitable for conversion into higher value derivatives, like esters and acetates, through simple reactions like esterification, transesterification, acetylation, etc.[6,8] As an example, cellulose acetate (CA) produced by acetylation of cellulose is an important cellulose derivative with a wide range of commercial applications in coatings, films, membrane separation, textile, pharmaceutical and cigarette industries.[9] Similarly, long chain fatty acids can be easily esterified to yield 'biodiesel' (FAME or FAAE), a first generation biofuel and glycerol could be converted into various commercially valued products like triacetin, acrolein, glycerol tertiary butyl ethers (GTBE), glycerol carbonate, telomers, branched alkyl ethers, propanediols and epoxides through simple reactions (Figure 1.2).[8]

It is a widely accepted fact in all chemical conversion processes that, next to feedstock, the selection of the catalyst plays the most important role as it can have a direct influence in the process economics. Catalytic conversion of biomass is not an exception. Accordingly, experts have identified '*catalysis*' as a key technology for the development of efficient biorefineries in the future.[1,2] However, the biggest challenge with the renewable feedstocks (biomass and its components) is their chemical structure (large critical/kinetic diameter, Table 1.1, Figure 1.3, functionalized structure, presence of heteroatoms such as oxygen, nitrogen and geographic variation in composition). Consequently, traditional industrial catalysts (e.g. zeolites, silica, especially microporous ones) often fail to convert these complex molecules efficiently and major research interventions are still needed concerning catalyst design, process design and optimization to improve conversion and make heterogeneous catalysis of biomass feasible in an industrial scale.

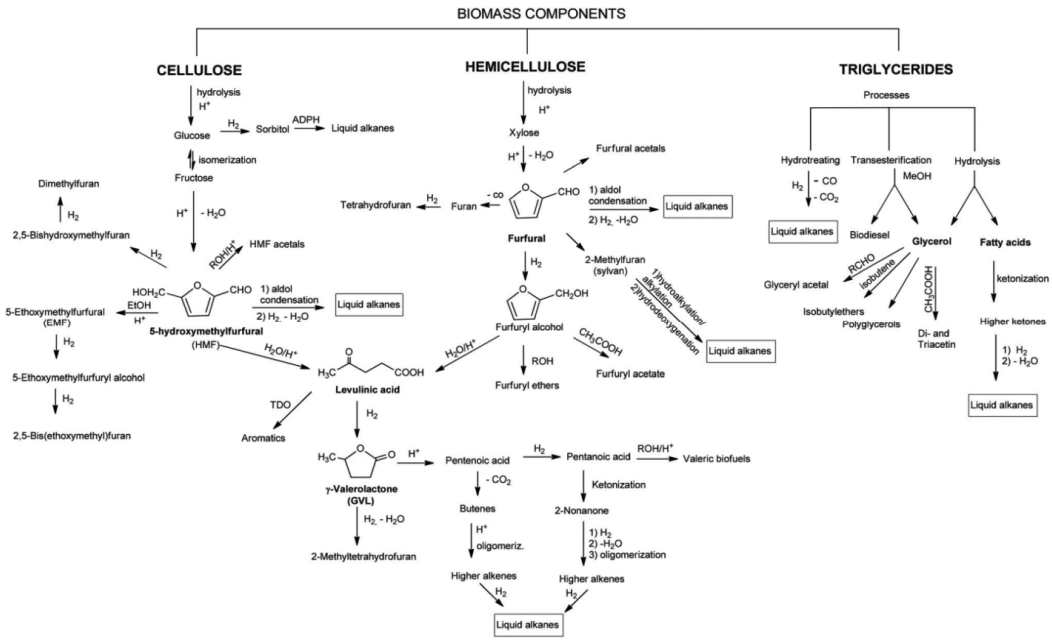

Figure 1.2. Catalytic options to convert biomass into valuable fuels, chemicals and fuel additives, adapted from ref. 6 with modifications.

Table 1.1. Dimensions of biomass components compared to pore dimensions of traditional solid catalysts

	Molecule dimensions (Å)			Pore dimensions of catalyst (Å)		
Feed molecule	**Critical diameter (width)**	**Maximum diameter (length)**	**Kinetic diameter, (r)**	**Catalyst**	**Pore size, (d_N)**	**Internal pore space (I_s)**
α-D-Glucose	8.417	8.583	8.6	H-ZSM-5	6.2, 6.3	6.36
β-D-Glucose	8.503	8.615	8.6	H-beta	7.4, 6.3	6.68
Cellulose	~100 (microfibril)	-	-	H-Y	8.1	11.24
Cellubiose	8.5	-	8.6	MCM-22	6.2	9.69
Xylitol	-	-	6.6	SAPO-34	5.0	7.37
Oleic acid	2.4		2.4			
Lauric acid	16.050	-	16.050			
Data compiled from refs. 10-13						

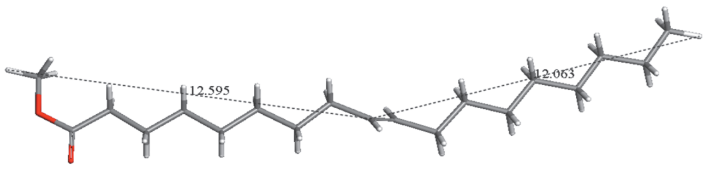

Figure 1.3. DFT optimized structure of oleic acid, adapted from ref. 13.

1.3. Carbon as catalyst

Approximately 90% of the chemicals in the industry are produced over heterogeneous catalysts using different petroleum feedstock as raw material (precursors). However, the same is not true for biomass based products as biomass processing at industrial level is still based on the homogeneous catalytic routes which are less selective and also produce large amounts of waste. This eventually leads to higher production costs and renders biomass based products less competitive in the market. Accordingly, the catalyst research for biomass conversion has been primarily focused on heterogeneous catalysis, in recent years. As already discussed, the investigated catalysts mainly include the traditional and chemically synthesized ones like zeolites, silica and metal supported (Pt, Pd, Au, Ni) zeolites, silica etc. Nevertheless, there are several drawbacks associated with these traditional catalytic systems in connection with their application in biomass conversion such as low catalytic activity, poor reusability, high material costs (use of expensive precious metals and support materials) and so forth, thus making them less attractive for industrial scale applications (in short, poor activity for the price). Thus, there is a particular need to develop active, robust and cheap catalytic systems capable of converting complex biomass molecules.[14]

In recent years, with the emerging concepts of green chemistry, the utilization of cheaper, green materials for chemical transformations has recently gained significant attention and several research groups have made efforts to develop a catalyst using inexpensive precursors such as biomass and waste materials. Among these, particularly the sulfonated carbons or $–SO_3H$ functionalized carbon catalysts have received considerable attention as a promising solid acid catalyst. These materials resemble H_2SO_4 in terms of acidity and catalytic activity, and also offer high operational stability (>240 °C and reusability), which make them versatile acid catalysts for the acid catalyzed reactions included in biomass transformation (Figure 2).[14-16] Functionalized carbon catalysts have been demonstrated to be amongst the most active and economically attractive catalysts

for biodiesel production, as reviewed by Konwar *et al.*.[14] Structurally they are comparable to active carbon and, like active carbon, they could also be prepared from any carbonaceous source, and their textural properties can easily be tuned by changing the carbonization/activation conditions. As a result, sulfonated carbons are much less expensive compared to traditional solids such as Amberlyst™, zeolites, sulfated zirconia etc. Besides, such activated carbon generated from inexpensive precursors could be a versatile support for the preparation of an inexpensive catalyst.[16]

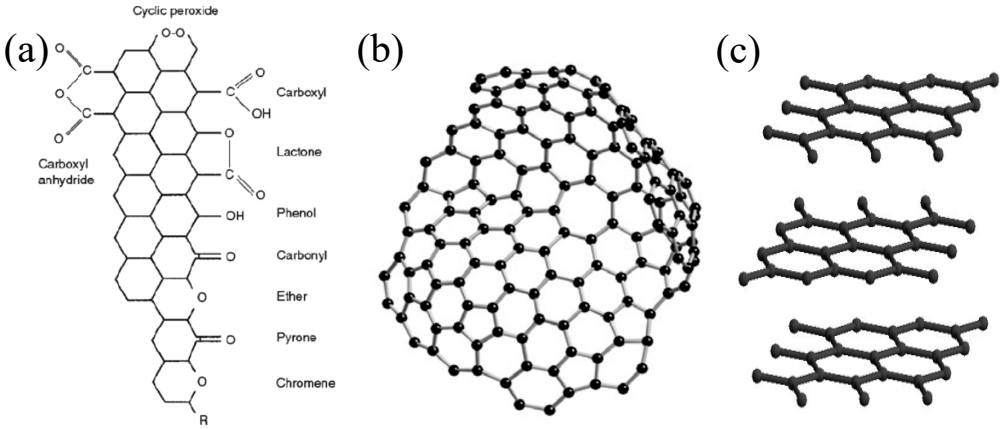

Figure 1.4. (a) Functional groups in activated carbon, (a) structure of activated carbons (also valid for amorphous carbon and biochar) and (b) structure of graphite, adapted from refs. 17-18.

Typically, activated carbons have a porous structure, usually with a relatively small amount of chemically bonded heteroatoms (mainly oxygen and hydrogen). Also, activated carbons have much higher specific surface area than other types of supports (>1000 m^2/g). Although a high specific surface area is usually considered advantageous in catalysis, in some cases it may be detrimental if it is confined in narrow micropores that are not accessible to the reactant molecules (Table 1.1). This is particularly important in processes where large biomass molecules, such as fatty acids, triglycerides and sugar oligomers are involved as in liquid phase reactions where diffusion of these reactants and their corresponding products may be hindered by the narrow porosity. The adsorptive properties of activated carbon are not only determined by its porous structure but also by its chemical composition. In graphite, with a highly oriented structure, the adsorption takes place mainly by the dispersion component of the van der Waals forces, but the random ordering of the imperfect aromatic sheets in the activated carbon results in incompletely saturated valences and unpaired electrons, and this will influence the adsorption behavior, especially for polar or polarizable molecules. In addition,

activated carbon is associated with such heteroatoms as oxygen and nitrogen (derived either from the starting material, activation process or post-treatment) and with the inorganic ash components. The presence of oxygen and hydrogen in surface groups can be up to 30 mol% H and 15 mol% O, which has a great effect on the adsorptive properties of the activated carbon. Some functional groups in active carbon supports are shown in Figure 1.4(a), while Figure 1.4(b)-(c) shows its structure in comparison to graphite. On the downside, the application of activated carbons is usually limited due to chemical reactivity in the presence of oxygen. This means that a conventional method of catalyst regeneration by burning of the coke away is not applicable. Moreover, active carbons are mechanically weak, which prevents their applications in fixed bed reactors and leads to generation of fines in slurry systems.[14,17,18]

1.4. Aim and scope of the research work

As a summary, the carbon based catalysts, such as sulfonated carbons, are promising catalysts in the realization of economical, carbon efficient biorefineries as they could be easily integrated into existing plants by using the abundant biomass wastes generated from biomass processing industries as catalyst precursors (de-oiled cakes, seed hulls, etc. from non-edible oil based biorefineries are particularly attractive due to the low carbohydrate content and limited uses). However, detailed information on structural and catalytic features of biomass derived carbon catalysts, as well as experimental data on reaction kinetics and mechanisms of the reactions catalyzed by such materials, are missing. Therefore, the main objective of the present thesis was to systematically investigate structural and catalytic features of these novel biomass derived catalysts (derived from nitrogen rich agro-industrial wastes generated from biodiesel production) and their catalytic behavior in selected acid catalyzed reactions involved in the valorization chain of the biomass components into industrially relevant products. For the sake of comparison, the catalytic activity of some commercial zeolites and mesoporous silica materials was also investigated in the same reactions. In this study, the liquid phase esterification of fatty acids, glycerol esterification, vegetable oil esterification/transesterification, cellulose saccharification, cellulose acetylation and glycerol acetylation were chosen as model reactions and investigated in batch mode. Herein, particular importance was given to understanding the reaction pathways (mechanisms) and kinetic aspects of the reactions in order to optimize the catalytic system, and to establish a correlation between the catalytic results and the physico-chemical properties of the new catalytic materials.

2. Experimental and analytical methods

2.1. Materials

Ortho-phosphoric acid (88%, Merck), oleic acid (technical grade, Merck), lauric acid (99%, Sigma), sulfanilic acid (99%, Merck), $NaNO_2$ (98%, Merck), H_3PO_2 (30-32%, SRL) anhydrous Na_2SO_4 (99.5%, Merck), $FeCl_2$ (99%, Sigma), $FeCl_3$ (99%, Sigma), H_2SO_4 (98%, Merck), HCl (35%, Merck), acetone (99.5%, Merck), methanol (99.9%, Merck), ethanol (99.9%, Merck), 1-Propanol (99.5%, Merck), glycerol (99.8%, Sigma), triacetin (99.9%, Sigma), diacetin (50%, Sigma), 1-ethyl-3-methylimidazolium chloride (>99%, Merck), microcrystalline cellulose (Sigma), Potato Starch (Pure, SRL), glucose (99.9%, Sigma), fructose (Sigma, 99.9%), 5-HMF (99%, Sigma), activated carbon (mesoporous, Sigma), heptane (HPLC, Sigma), pyridine (HPLC, Merck), FAME mix (Supelco), methyl heptadecanoate (99%, Supelco), N-methyl-N-trimethylsilyltrifluoroacetamide (98%, Sigma), ASTM® D6584 Individual Standard Solution (Supelco) and Internal Standards Kit (Supelco) were purchased from commercial sources and used as received.

2.2. Catalysts

2.2.1. Carbon based acidic catalysts

In this work the precursors or raw material used for preparation of carbon catalysts were de oiled waste cake (DOWC, a by-product from processing of non-edible oil seeds used in biodiesel production)[19] and commercial potato starch. *Jatropha curcas* (J), *Pongamia pinnata* (P) and *Mesua ferrea* L. (M) seed DOWC, left after oil extraction by Soxhlet method were collected as end wastes from Biofuel and Biomass conversion Laboratory, Department of Energy, Tezpur University (Assam, India). Prior to carbonization/activation experiments DOWCs were ground, sieved and particles of size <250 μm collected and storaged in a desiccator (Chemical composition, Table 2.1). Herein, three different approaches (see below) were adopted for the preparation of catalytic materials with different textural and acidic properties. The detailed synthesis procedure, characterization and results of catalytic tests are reported in publications [**I, II, III, IV**].

Table 2.1. Composition of raw material (DOWC)

Properties	DOWC		
	M	P	J
Elemental analysis (Wt %)			
C	48.6	43.7	42.5
H	7.4	6.6	5.4
N	3.6	3.2	10.7
O a	40.3	46.5	41.4
S	-	-	-
Biochemical analysis (Wt %)			
Protein	20.2	22.8	61
Carbohydrate	79.8	77.2	39
Lipid	trace	trace	trace
Proximate analysis (Wt %)			
Moisture	4.1	3.8	4.4
Volatile matter	82.6	80.1	74.1
Fixed carbon	8.4	11.9	16.6
Ash	4.8	4.1	4.9

[a] based on difference (ash free basis); n.d = not determined.

2.2.1.1. Mesoporous sulfonated carbon

The mesoporous sulfonated carbon catalysts were prepared by the sulfonation of activated carbon (AC) derived from J, P or M DOWC residues (obtained by phosphoric acid activation) with 4-benzenediazoniumsulfoante (4-BDS) or conc. H_2SO_4, further details about the carbonization conditions and catalyst preparation methods can be found in the publications [**I, II, III, IV and VI**]. Briefly, in a typical process, approximately 10 g DOWC (particle size <250 μm) biomass pre-soaked in 50 % (v/v) ortho-phosphoric acid for 24 h were activated at 450, 500 and 600 °C to obtain the active carbons. The resulting carbons thoroughly washed with hot deionised water and subjected to sulfonation. For comparison, commercial mesoporous carbon was also similarly sulfonated with 4-BDS.

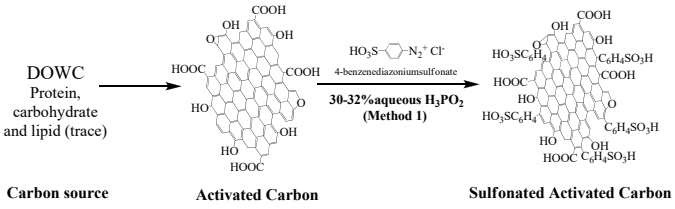

Scheme 2.1. Preparation of sulfonated carbons by functionalization of 4-BDS or radical route.

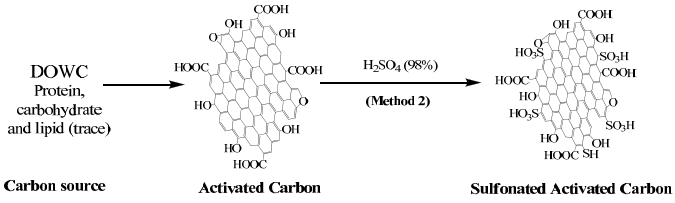

Scheme 2.2. Preparation of sulfonated carbons by H_2SO_4 or direct sulfonation route.

In a typical 4-BDS sulfonation, sulfanilic acid (5.2 g) was dispersed in 1 M HCl aqueous solution (300 mL) in a three-necked flask. The flask was moved into an ice water bath, and the temperature was controlled at 3–5 °C with continuous stirring. Thereafter, 10% excess 1M of $NaNO_2$ (33 mL, aqueous solution) was added dropwise, a clear solution was obtained after all the $NaNO_2$ was added. After stirring for another 1 h at the same temperature, the white precipitate of 4-

benzenediazoniumsulfonate formed was filtered off, washed with deionized water and moved into a three-necked flask with deionized water (200 mL) and ethanol (120 mL). Then, active carbon (1 g) was added maintaining the temperature at 3–5 °C. Subsequently, 30-32 % H_3PO_2 aqueous solution (100 mL) was added. After stirring for 30 min, another 50 mL of H_3PO_2 aqueous solution was added and allowed to stand for another 1 h or until the evolution of N_2 had ceased with occasional stirring (Scheme 2.1). The obtained sulfonated carbons were thoroughly washed with acetone, deionised water, dried in vacuum overnight, ground to powder and marked as JACS, PACS and MACS (series I, obtained from different raw materials J, P and M), respectively. Another series of samples were denoted AC450S, AC500S and AC600S (series II) were obtained from P biomass derived active carbons obtained at different temperatures. In the H_2SO_4 sulfonation method, the sulfonated catalysts were prepared by the direct treatment of DOWC based AC obtained above with 98% H_2SO_4 at elevated temperatures according to a modified method of Hara *et al.*[15,16] Briefly, 20 g H_2SO_4 (98%) was mixed with 1 g MAC and refluxed at 180 °C for 8 h. The obtained black products (marked as $MACH_2SO_4$) were filtered, thoroughly washed with acetone, deionized water and then dried in vacuum overnight (Scheme 2.2).

2.2.1.2. Non-porous sulfonated carbon

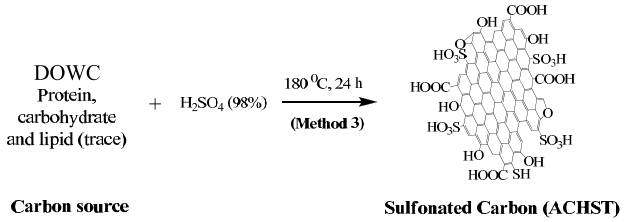

Scheme 2.3. Preparation of sulfonated carbons by one step hydrothermal route.

The non-porous sulfonated carbons were prepared by direct (one-step) hydrothermal sulfonation of DOWC with conc. H_2SO_4 (98%). In a typical process, 1 g deoiled cake was mixed with 5 g conc. H_2SO_4 and heated in a 50 mL Teflon-lined autoclave at 180 °C for 24 h (Scheme 2.3). The resulting material was thoroughly rinsed with hot deionized water, dried and ground to powder (ACSHT and MACHT). Further details of the synthesis process can be found in publication [**I,II**].

2.2.1.3. Magnetically separable sulfonated composite catalyst

The $–SO_3H$ functionalized magnetic FeC composite catalyst was prepared in three steps. Firstly, the magnetite (Fe_3O_4) particles were prepared by a coprecipitation method from a 0.4 N HCl solution containing $FeCl_3$ and $FeCl_2$ (Fe^{+2}/Fe^{+3} molar ratio was 0.5) [16]. 25 mL of the resulting solution was added dropwise to 250 mL of 1.5 N NaOH solution under vigorous stirring. To stabilize the nanoparticles (NP) 100 µl of oleic acid was also added. Finally, impurity-free, oleic acid-stabilized magnetite NPs were obtained by repeated centrifugation and washing with deionised water. In the next step, carbon coated magnetite NP composite was pretreated by hydrothermal treatment of 5 g of the NPs in 100 mL deionised water containing 5 g starch in a 200 mL Teflon-lined autoclave at 180 °C for 24 h. Finally, the carbon coated magnetite NP were activated at 500 °C and subsequently sulfonated with freshly prepared 4-BDS to obtain the magnetically separable sulfonated composite catalyst (marked FeCS) **[V]**.

2.2.2. Acidic zeolites and mesoporous silica (reference catalysts)

The commercial zeolites H-Y [SiO_2/Al_2O_3=12, surface area=884 m^2g^{-1}, acidity=0.83 $mmolH^+g^{-1}$] and H-ZSM-5 [SiO_2/Al_2O_3=23, surface area=443 m^2g^{-1}, acidity=1.14 $mmolH^+g^{-1}$], H-beta 25 [SiO_2/Al_2O_3=25, surface area=589 m^2g^{-1}, acidity=0.781 $mmolH^+g^{-1}$], H-beta 150 [SiO_2/Al_2O_3=150, surface area=546 m^2g^{-1}, acidity=0.715 $mmolH^+g^{-1}$] and H-beta 300 [SiO_2/Al_2O_3=300, surface area=661 m^2g^{-1}, acidity=0.167 $mmolH^+g^{-1}$] were purchased from zeolyst International in NH_4^+ form and calcined at 450 °C for 24 h prior to use. The calcination of the zeolite catalysts were carried out using a ceramic plate in a muffle oven in stagnant atmospheric air. The H-form of the H-Beta-150 and H-Beta-300 zeolite catalysts were obtained using step calcination procedure as follows: 60 min – 250 °C, 40 min – 250 °C, 50 min – 450 °C, 240 min – 450 °C and 100 min – 25 °C **[I,III,IV,V]**. The mesoporous zeolites MCM-41 [SiO_2/Al_2O_3=20, surface area=944 m^2g^{-1}, acidity=0.112 $mmolH^+g^{-1}$] and MCM-48 [SiO_2/Al_2O_3=n.a, surface area=714 m^2g^{-1}, acidity=0.174 $mmolH^+g^{-1}$] were synthesized and reported by Käldström *et al.*[20] and also used in this study as reference catalysts **[I,III]**. The specific details of the synthesis and characterizations of these materials can be found elsewhere.[20]

2.3. Catalyst characterization

The X-ray powder diffraction patterns of carbon samples were recorded on a Rigaku miniflex diffractometer (Cu-Kα radiation, λ=1.5406 Å) in 2θ range 10–70 at a scanning rate of 4 degreemin^{-1}. The morphological features of the sulfonated carbons were studied by Scanning electron microscopy using a Zeiss Leo Gemini microscope operating at 20kV. The elemental composition and the corresponding element mapping distributions of the carbon materials were obtained on a Jeol, JSM-6290LV instrument operating at 20kV by energy-dispersive X-ray analysis (EDX). The elemental composition of non-sulfonated materials and the carbon sources were determined by organic elemental analysis (OEA) on a Thermo Scientific FLASH 2000 apparatus. Transmission electron micrographs were recorded on a Jeol JEM-2100 electron microscope operating at 200 kV. The resolution was around 0.4 nm. Samples were suspended in ethanol and deposited instantly on a copper grid for analysis. The elemental composition and the oxidation state of surface functionalities, including the presence of -SO_3H and phosphates groups were evaluated by X-ray photoelectron spectroscopy on a Kratos Axis Ultra DLD spectrometer with a monochromatized Al Kα X-ray source that was operated at 14 kV, 300 W. The analyzer pass energy was 17.9 eV and the energy step was 0.1 eV. The vacuum chamber base pressure was 10^{-9} mbar. FT-IR spectra were recorded in KBr pellets on a Nicolet (Impact 410) FT-IR spectrophotometer. On occasions FT-IR were also obtained on a Perkin ELmer in ATR mode. The Laser Raman micrographs of carbon samples were obtained on a RenishawInVia laser Raman microscope using 514.5 nm laser. The specific surface area, pore size and pore volume of the carbon materials were determined by means of N_2 physisorption at liquid nitrogen temperatures on a Carlo ErbaSorptomatic1990 instrument. The specific surface area (S_{BET}) was determined by the BET equation (P/P_0 = 0.05–0.3). The pore size distribution was determined from the desorption branch of the isotherm using the Barrett-Joyner-Halenda (BJH) method. The micropore volume was calculated with the Dubinin—Radushkevich equation. All samples were pre-treated at 150 °C while degassing (~0.1 Pa). The thermal stability of the catalytic materials were investigated by thermo gravimetric analysis (TGA-50, Shimadzu) from room-temperature to 550 °C at a ramping rate of 10 °C min^{-1} under nitrogen flow (UHP grade).

The surface acidic properties of carbon materials were measured by the ammonia temperature-programmed adsorption-desorption (AutoChem 2910, Micromeritics) and compared

with the results obtained by titration. 0.1 g sample was placed in an adsorption vessel (U-shaped) and activated at 120 °C in He flow for 2 h (heating rate 10 °Cmin^{-1}). Then the sample was cooled to 120 °C in He flow. At this temperature, 5% NH_3 in He was passed through the sample for 1 h followed by cooling to 100 °C in He flow. TPD was carried out from 100 to 500 °C at a heating rate of 10 °Cmin^{-1} with He flow rate of 35 mLmin^{-1}. After each TPD measurement, the amount of ammonia adsorbed was determined form the calibration curve obtained from varying volumes of ammonia in He. Further, the acid site densities of the catalytic materials were also determined by acid-base titration method as reported previously.[19]

2.4. DFT calculations

In order to correlate the shape selectivity effects due to catalyst pore structures in the investigated reactions, molecular dimensions of reactant and product molecules were determined by density functional (DFT) calculations performed using DNP (double numerical plus polarization) basis set implemented in DMol^3 package whenever such data were not available in literature. Geometry optimizations and frequency analysis were done by treating the exchange–correlation interaction with generalized gradient approximation (GGA) using Becke–Lee–Yang–Parr (BLYP) exchange–correlation functional. The DNP basis set is comparable to Gaussian 6-31G**, but DNP is more accurate than a Gaussian basis set of the same size. The geometries of the molecules were optimized without imposing symmetry constraints using all electron spin-unrestricted calculation, indicating electronically open shell system. Inversion iterative subspace (DIIS) approach was used in order to speed up SCF convergence. Molecule *lengths* were calculated as the distance between the two farthest-apart atoms along a line orthogonal to the critical diameter, plus an estimate of the estimate of the van der Waals radii of the hydrogen (1.2 Å) or oxygen (1.52 Å) atoms involved. On the other hand, *critical diameter* is the internuclear distance between the two nuclei that intersected the surface of the smallest possible cylinder containing all nuclei plus an estimate of the atoms' radii **[II]**.

2.5. Evaluation of catalytic properties

In this investigation, all the reactions were carried out in liquid phase in batch mode using glass reactors and on occasions with a pressurized autoclave equipped with stirring and sampling port. Selected experiments were also performed with 2 mL mini-autoclaves (Figure 2.1-2.2).

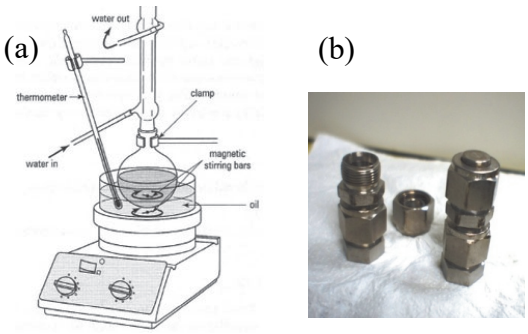

Figure 2.1. (a) Standard batch type glass reactor and (b) 2 mL mini-autoclaves.

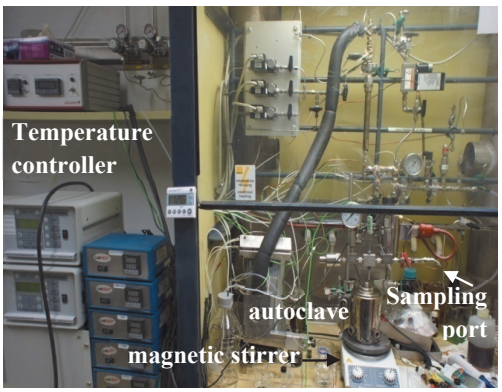

Figure 2.2. Pressurized autoclave (35 mL) equipped with magnetic stirring and sampling port.

2.5.1. Cellulose hydrolysis

Hydrolysis reactions were performed in batch mode in 2 mL mini autoclaves on a hot plate at temperatures of 100 °C, 120 °C and 150 °C, respectively under autogenous pressure according to the conditions described by Onda *et al.*[21] In brief, 0.01 g of cellulose, 0.01 g of catalyst (particle size <200 μm) and 1 mL distilled water were loaded into the autoclaves, heated to desired reaction temperature and held at this temperature for 24 h. After completed reaction, the mini-reactors were immediately cooled under tap water to quench the reaction. The reaction mixture was taken out and centrifuged to separate the solids (containing catalyst and the unreacted cellulose particles). Thereafter, the liquid phase was analyzed by means of High-Performance Liquid Chromatography, (Hitachi HPLC LaChromUltra) equipped with Aminex HPX-87C column **[I]**.

2.5.2. Fatty acid (oleic) esterification with monohydric alcohols

Esterification reactions were performed under atmospheric pressure in a 100 mL three-necked flask equipped with a magnetic stirring and a digital thermometer in an oil bath. Reactions were

performed with technical grade oleic acid using 3 wt% catalyst loading at methanol reflux temperature with varying alcohol to acid molar ratios (5-30). In a typical reaction, 0.15 g catalyst (particle size <200 μm, outgassed at 150 °C) was added to an appropriate amount of methanol/ethanol/2-propanol and heated to 64 °C and followed by an addition of 5 g preheated oleic acid with vigorous stirring (300 rpm) for 10 h. In order to investigate catalyst stability, reactions were also conducted with the spent catalyst which was recovered by filtration and subsequently washed with methanol **[I]**.

2.5.3. Simultaneous esterification and transesterification of vegetable oil

Reactions were performed in batch mode in an autoclave (V_i = 35 mL) equipped with magnetic stirring, digital temperature controller and a sampling valve under autogenous pressure (Figure 2.1). All experiments were performed with 10 g of moisture free feedstock oil (I, II or III) using 0.5 g catalyst loading and with varying amounts of methanol. The catalyst amount was fixed at 5 wt % of oil (0.5 g) based on our earlier work.[19] In brief, the reactants, i.e. the feedstock oil, methanol as well as the catalyst, were first added to the reactor. Before starting any experiment, the reactor was flushed with nitrogen (99.99%) to remove moisture and any other reactive gases. The reaction mixture was then heated to the desired temperature under autogenous pressure and the actual reaction proceeded with vigorous stirring at 1400 rpm for 1440 min (24 h). A summary of the experimental conditions are given in the publication [**II**]. The progress of the reaction was monitored by periodically withdrawing small samples from the reaction mixture that were analyzed with chromatography. To conduct catalyst reuse tests, spent catalyst was recovered by filtration after which it was thoroughly washed with acetone and ethanol, followed by drying under vacuum overnight at 80 °C. The spent catalyst was reused as before without any change of reaction parameters **[II]**.

2.5.4. Glycerol acetylation

Catalytic reactions were performed in batch mode in a 50 mL, three-necked flask equipped with a thermometer and a condenser. Stirring was performed magnetically with a stirr bar. In all catalytic experiments, particles of size <63 μm were used to reduce mass transfer limitations. In a typical reaction, the mixture of 0.25 g catalyst (~5 wt% of glycerol) and 5 g glycerol (~55 mmol) were heated to the desired reaction temperature followed by an addition of acetic anhydride. The molar

ratio of anhydride to glycerol was varied from 1:1 to 1:5. For comparison, reactions were also performed using acetic acid at 120 °C **[III]**.

2.5.5. Fatty acid (lauric, oleic) esterification with glycerol

Reactions were performed in batch mode under atmospheric pressure within the temperature range of 100-150±5 °C in a 100 mL three-necked flask equipped with a magnetic stir bar, a sweeping gas connection (N_2 at 5 $mLmin^{-1}$, to remove water formed during esterification) coupled to a temperature controlled oil bath. To ensure uniform mixing of the catalyst particles, and to minimize the influence of external mass transfer effects, the stirring speed was set at 650 rpm. Furthermore, small catalyst particles in the size range of 5-70 μm were used in order to suppress internal mass transfer limitations. In a typical reaction, 0.5 g of pre-dried catalyst (5 wt% of the glycerol mass) was added to 10 g glycerol and heated to the desired reaction temperature under vigorous stirring. When the preset temperature was reached, an addition of fatty acid (lauric or oleic, corresponding to fatty acid-to-glycerol molar ratio = 1) was commenced **[IV]**.

2.5.6. Cellulose acetylation

Catalytic reactions were performed in a 50 mL two-necked round bottom flask equipped with magnetic stirring and reflux condenser in a temperature controlled oil bath. In a typical process 1 g (~6.1 mmol AGU) cellulose (particle size <70 μm and vacuum dried at 70° for 24 h), 2.8-5.7 g acetic anhydride, and 0.25–1 g catalyst (size range 7–70 μm) were heated at 80 °C with constant mechanical stirring for 12–24 h. In order to ensure uniform mixing of the cellulose with catalyst particles, the stirring speed was set at 1000 rpm in all experiments. The resulting viscous liquid (product) was cooled to room temperature, diluted with 40 mL acetone/DMSO (approximately 5 times by volume) and centrifuged at 4000 rpm for 35 min to separate the catalyst particles. The obtained liquid mixture was poured into 50 mL of 50% (v/v) ethanol and stirred for 30 min to precipitate CA. Finally, the acetylated product (CA) was filtered, thoroughly washed with deionised water in order to remove excess acetic anhydride and acetic acid formed during the reaction and dried in vacuum at 70 °C **[V]**.

2.6. Reaction product analysis

2.6.1. Analysis of cellulose hydrolysis products

The liquid phase of the cellulose saccharification reactions was analyzed by means of High-Performance Liquid Chromatography, (Hitachi HPLC LaChromUltra) equipped with Aminex HPX-87C column. The column was connected with a refractive index (RI) detector where dilute solution of calcium sulfate ($CaSO_4$, 1.2 mM) was used as mobile phase. Liquid samples were filtered through 0.2 μm filter membrane and directly injected to the HPLC. The individual products were identified using commercially available standards of glucose, fructose, mannose, xylose, 5-HMF and furfural, and the concentration of specific product determined from calibration curves obtained with these standards. The final yield (mol-C%) was calculated according to following the equation reported by Onda *et al.*[21]

$$\text{Yield (mol} - \text{C\%)} = \frac{\text{mol of glucose/HMF} \times 6}{\text{mol of C in the cellulose (elemental analysis)}} \times 100 \quad (2.1)$$

Conversions were based on the weight difference between unreacted cellulose and cellulose fed into the reactor, and catalyst turnover frequency (TOF) was expressed as moles of glucose formed per mole of acid site per hour. Here, the amorphous cellulose substrate was prepared by ionic liquid pretreatment as follows: In a typical process, 0.5 g microcrystalline cellulose was dissolved in 9.5 g 1-ethyl-3-methylimidazolium chloride ionic liquid and heated at 130 °C for 1.5 h with occasional stirring. Cellulose was regenerated by adding hot distilled water into the resulting solution, separated by filtration and dried at 100 °C **[I]**.

2.6.2. Analysis of products of fatty acid (oleic) esterification with monohydric alcohols

2.6.2.1. Acid value of product

The progress of fatty acid esterification was monitored by direct titration method as follows: at selected time intervals, 0.1 mL aliquots were taken from the reaction mixture and centrifuged at 6000 rpm for 3 min to separate the catalyst particles. The acid value of the lower ester layer was determined by titration (in triplicates) after removal of excess methanol with standard KOH (0.01 mol L^{-1}) solution. The conversion of acid was calculated as:

$$C_{Est}(\%) = \frac{(C_i - C_t)}{C_i} \times 100 \quad (2.2)$$

where, C_i and C_t are the acid value at 0 min and t min respectively. The rate constant, 'k' was calculated from the slope of time (t) vs. ln(1-(C_{Est}/100)) plots. The TOFs were calculated using 'k' values according to the equation below.

$$TOF = \frac{k \times C}{n_S} \quad (2.3)$$

where, C denotes the amount of oleic acid (in mmol) loaded into the reactor and n_s is the amount of strong acid (-SO_3H) sites on the catalyst loaded into the reactor **[I]**.

2.6.2.2. ^{1}H-NMR analysis of fatty acids and esters

The ester formation and aromatic leaching were also confirmed by ^{1}H-NMR analysis of reaction mixtures following completion of reaction on a Jeol JNM-ECS400 NMR spectrometer at 25.5 °C using $CDCl_3$ as a solvent and TMS as the internal standard **[I]**.

2.6.3. Analysis of products of simultaneous esterification and transesterification

2.6.3.1. Silylation-gas chromatography

The progress of the reaction was monitored by periodically withdrawing small samples from the reaction mixture that were analyzed chromatographically. In order to make the components of reaction mixture (fatty acids, mono and diglycerides) more volatile, the samples were silylated with N-Methyl-N-trimethylsilyltrifluoroacetamide (MSTFA) reagent according to a modified ASTM-6584 method. Briefly, 0.1 mL samples of were taken from the reactor at selected time intervals, dried over N_2 stream. In the next step, 10 mg sample was accurately weighed into 10 mL vials, followed by an addition of 200 µl pyridine and 50 µl MSTFA reagent. After adding MSTFA, the samples were allowed to stand at room temperature for 30-45 min for completion of the reaction, and further diluted with reagent grade heptane to make concentration of (~10 $mgmL^{-1}$). The commercially obtained stock standards, at concentrations specified in the ASTM method, were also similarly derivatized to their tetramethylsilane (TMS) forms with an excess MSTFA to make calibration curves. These final mixtures were directly injected into a HP series II Gas chromatograph equipped with a FID detector and a Zebron ZB-5HT Inferno column (30 m length; 0.30 mm internal diameter; 0.10 µm film thickness) according to the ASTM D6584 method. The

column temperature was held at 50 °C hold 1 min, 15 °Cmin^{-1} to 180 °C, 7 °C/min to 230 °C, 30 °Cmin^{-1} to 380 °C and held for 5 min. Helium was used as the carrier gas at a flow rate of 3 mLmin^{-1} **[II]**.

2.6.4. Analysis of the glycerol acetylation product

For product analysis at selected time intervals, 0.2 mL aliquots were taken from the reaction mixture and immediately quenched by adding 4 mL methanol, centrifuged at 6000 rpm for 3 min to separate the catalyst particles and analyzed by GC-FID on HP series II chromatograph to determine product distributions. The individual products were identified by comparison with commercially available standard compounds, and the yields were calculated using calibration curves obtained with these standards. Further details can be found in publication **[III]**.

2.6.5. Analysis of products of fatty acid (lauric, oleic) esterification with glycerol

The progress of the reaction was monitored by periodically analyzing the reaction mixture. Briefly, 0.1 mL aliquots were periodically withdrawn from the reaction mixture, dried over N_2 stream and analyzed by gas chromatography (GC) on a TRACE™ 1300 (Thermo Scientific) gas chromatograph equipped with FID detector and Agilent (Select Biodiesel for glycerides), column (30 m length; 0.30 mm internal diameter; 0.10 µm film thickness). The sample preparation and analysis procedures are similar to silylation-gas chromatography discussed above in section 2.6.3.1.The fractional conversion was expressed with respect to the fatty acid (FA) concentration in the reaction mixture determined by external standard method from calibration curves obtained with FA.

$$\text{Conversion (\%)} = \frac{\text{CFA}_0 - \text{CFA}_t}{\text{CFA}_0} \times 100 \quad (2.4)$$

The selectivity of a specific glyceride mono- (MG), di- (DG) or triglyceride (TG) was expressed by the molar ratio of the glyceride to all the glycerides. The initial rate (k) of FA conversion/reaction, MG and DG formation were calculated from the slope of time (t) vs. ln(conc.) plots of corresponding components. The turnover frequencies (TOF) were calculated using 'k' values according to the equation below.

$$\text{TOF} = \frac{k \times \text{CFA}}{n_s} \quad (2.5)$$

where, CFA denotes the amount of fatty acid (in mmol) loaded into the reactor and n_s is the amount of active acid sites on the catalyst loaded into the reactor **[IV]**.

2.6.6. Analysis of cellulose acetylation product

2.6.6.1. FT-IR (ATR) and NMR spectroscopy

The final product (CA) was also analyzed by FT-IR (ATR) and NMR spectroscopy. DS of product was calculated using ^{1}H-NMR data as follows:

$$\mathrm{DS} = \frac{7 \times \mathrm{A_{acetate}}}{3 \times \mathrm{A_{AGU}}} \tag{2.6}$$

where, $A_{acetate}$ is the area of the methyl signals, and A_{AGU} is the area of the proton signals of the AGU unit. The DS analyses were performed as triplicates. To prepare CA film, CA was redissolved in CH_2Cl_2, filtered and the filtrate was evaporated on a wash glass under vacuum at 50 °C when a transparent CA film formed upon complete drying **[V]**.

2.6.6.2. Determination of the product yield

The isolated product yield was calculated based on the complete substitution of cellulose using the equation below:

$$\begin{aligned}\text{Yield (\%)} &= \frac{\mathrm{m_{CA}(g)}}{\mathrm{m_C}/162 \times 291} \times 100 \\ &= \frac{\text{Actual yield of CA (g)}}{\text{Theoritical yield of CA (g)}} \times 100\end{aligned} \tag{2.7}$$

where, m_{CA}, m_C represent the mass of acetylated product (or acetylated product+catalyst), cellulose (or cellulose+catalyst) and 162 and 291 represent the mass of anhydroglucose (AGU) unit of cellulose and cellulose triacetate respectively **[V]**.

3. Results and discussion

3.1. Catalyst characterization results

3.1.1. Catalyst structure and surface properties [I,III,IV,V]

The structural determination/analysis of the synthesized novel carbon catalysts were based on XRD (data not shown), laser Raman (data not shown), FT-IR (Figure 3.1) and XPS (Figure 3.2, Table 3.1) analysis.

Table 3.1. Deconvolution of XPS peaks of the carbon materials (selected) obtained from DOWC

Peak	Assignment	JAC Position (eV)	JACS Position (eV)	PAC Position (eV)	PACS Position (eV)	MAC Position (eV)	MACS Position (eV)	$MACH_2SO_4$ Position (eV)
C1s	C=C, sp2	284.6	284.6	284.4	284.3	284.3	284.3	284.5
	C=N sp2 and C=C sp3	285.7	285.8	285.6	286	285.5	285.7	286
	C-O	287.2	287.3	-	-	286.8	287.1	287.2
	C=O	288.4	-	287.1	287	288.1	-	-
	COO	-	288.8	288.2	288.1	289	288.8	288.9
	satellite	289.7, 291.6	291.1	290.3	290.6	290.9	291	291
O1s	=O	530.7	530.8	530.5	530.8	530.4	530.9	530.7
	-O-	532.8	532.5	532.4	532.5	532	532.6	532.1
	$O + H_2O$ (chemisorbed)	536	534.5	536.8	534.6	533.5	-	533.3
N1s	pyridinic N	398.4	398.3	398.2	398.1	398.3	398.2	398.2
	pyrrolic N	400	400	399.9	399.8	399.8	399.9	400.1
	quaternary N	401.2	401.8	401.2	401.3	400.9	401.3	401.5
	N oxide of pyridine N	403.1	-	403.1	403	404.2	402.6	403.3
P2p	PO4	133.4	134.5	133.4	133.5	133.4	133.4	133.4
S2p	–SH	-	-	-	-	-	-	163.8
	$C\text{-}SO_3^-$	-	167.2	-	167.2	-	167.3	-
	SO_4^{2-}or $-SO_3H$	-	168.1	-	168.3	-	168.3	167.1

The occurrence of an amorphous carbon structure with randomly oriented polycyclic aromatic carbon sheets was supported by the characteristic XRD: broad (002) and (101) diffraction peaks at 2θ=35-50° and 2θ=15-30° and Raman peaks: D-band vibration at 1339 cm^{-1} and G-band vibration at 1600 cm^{-1}; while, FT-IR and XPS analysis confirmed the presence of –COOH, –OH,

phosphate and –SO_3H /–$PhSO_3H$ functionalities on the surface of novel catalysts and resembled sulfonated carbon catalysts reported in earlier works.[13-16]

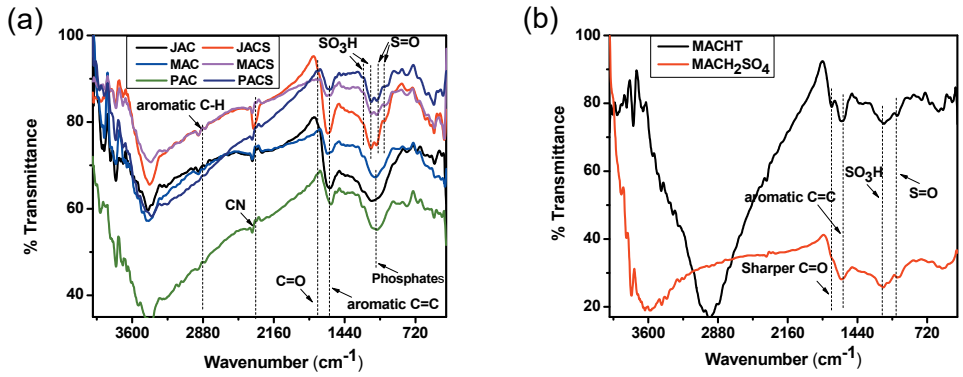

Figure 3.1. FT-IR spectra of catalytic materials (selected) obtained from DOWC biomass: (a) prepared by method 1 (sulfonation with 4-BDS) with their non-sulfated forms (AC) and (b) prepared by conc. H_2SO_4 treatment (method 2 and 3).

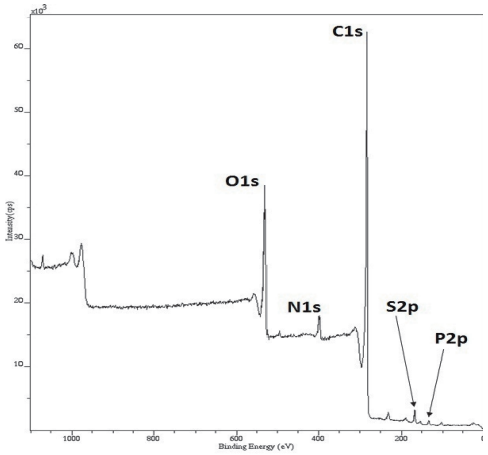

Figure 3.2(a). A wide angle XPS spectrum of a representative sulfonated active carbon catalyst PACS showing the O1s, C1s, N1s, S2p peak and P2p peaks.

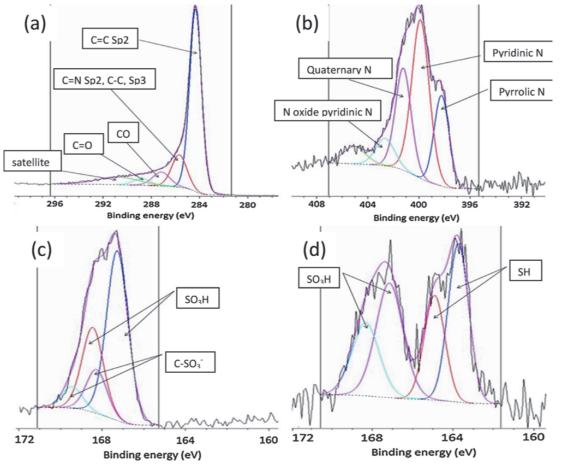

Figure 3.2(b). Deconvolution of XPS spectra (a) C1s peak, (b) N1s peak, (c) S2p peak and (d) S2p peak of $MACH_2SO_4$.

Also, the deconvolution results of high-resolution XPS spectra (C1s, N1s, O1s, S2p and P2p regions) showed the existence of several other functionalities: PO_4 or polyphosphates, nitrogen derivatives (Pyridinic, -NH_2, Pyrrolic, quartanery, N-Oxide) and –SH on the catalyst surface

(Table 3.1). Indeed, a strong co-relation was found to exist between the composition of starting material (DOWC) and preparation method on catalyst structure as well as textural characteristics. Detailed descriptions of the characterization results of these materials can be found in the publication [**I, II, III**]. Overall, the characterization results indicate a very complex structure for the herein reported DOWC biomass derived novel sulfonated carbon catalysts being different from the typical non-porous sulfonated carbons derived from carbohydrate, sugar or resin by Hara *et al*. method (pyrolysis followed by sulfonation with conc. or fuming H_2SO_4).[15,16]

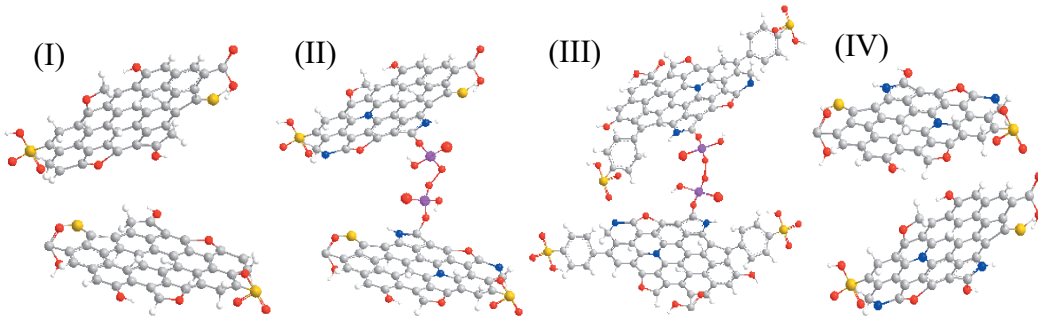

Figure 3.3. Plausible structure for the structural units of (I) the typical carbohydrate or sugar or resin based sulfonated carbons, based on Hara *et al.* method[15,16] and the sulfonated carbon catalysts prepared herein from DOWC by (II) method 2, (III) method 1 and (IV) method 3. Notation, represent C, N, O, S, P and H, respectively.

Structurally, these multifunctional materials are related more to the N-doped carbons or carbon nitrides rather than amorphous or active carbons.[22] Hence, in contrast to the typical sulfonated catalyst where the basic structural unit is simply a flexible aromatic carbon or graphene sheet functionalized with –OH, –COOH and $–SO_3H$ groups (I), the structural unit of sulfonated carbons obtained from the protein (nitrogen) rich DOWC resembles a flexible carbon nitride sheet which has been extensively functionalized with –OH, –COOH, phosphates (PO_4) and $–SO_3H$/$–PhSO_3H$ groups. The prepared catalytic materials may adopt any one of the three structures II or III or IV depending on the method of preparation (Figure 3.3). The density and nature of surface functional groups are directly affected by carbonisation conditions (temperature, use of activating agent etc.) and sulfonation method. Here, the H_2SO_4 treated and phosphoric acid activated DOWC (method 2) will take up structure II (with $–SO_3H$), while the materials prepared by method 1 (4-BDS

treated) will adopt structure III (with -$PhSO_3H$), and the hydrothermally sulfonated and carbonised materials (method 3) will take up structure IV.

Table 3.2. Elemental composition and the textural properties of the novel carbon catalysts

Catalyst	Element				[a]Surface area	[b]Pore volume	[c]Pore diameter	I_D/I_G	[e]L_a
	N (wt%)	**C** (wt%)	**H** (wt%)	**S** (wt%)	$m^2g_{cat}^{-1}$	$cm^3g_{cat}^{-1}$	nm		Nm
JAC	7.4	53.38	3.12	-	423	0.32	3.93	0.79	5.56
PAC	3.1	78.6	2.2	-	914	0.77	6.7	0.64	6.72
MAC	3.2	77.3	2.82	-	786	0.63	4.4	0.86	5.07
AC450				-	836	-	3.70	-	-
AC500				-	820	-	3.72	-	-
AC600	2.15	74.23	3.2	-	890	-	3.92	-	-
CAC	n.d	n.d	n.d	-	201	0.14	7.7	-	-
Post sulfonation materials									
method 1(Scheme 2.1)									
JACS	5.46	46.75	4.75	2.26	93	0.23	3.9	0.86	4.9
PACS	2.84	70.91	3.08	2.69	483	0.46	4.8	0.66	6.68
MACS	3.24	72.82	3.14	2.41	468	0.39	4	0.9	4.85
MAC-SO_3H	4.49	54.65	3.73	2.35	690	0.61	4.1	0.86	5.07
AC450S	2.57	70.79	3.01	2.12	533	-	3.87	-	-
AC500S	2.49	69.92	3.08	2.63	483	-	3.84	-	-
AC600S	2.15	68.38	3.19	2.91	352	-	3.71	-	-
CACS	0.40	73.53	2.97	1.7	119	0.07	5.5	-	-
ACSO3H	2.90	70.21	3.12	2.63	483	0.45	4.7	-	-
method 2 (Scheme 2.2)									
$MACH_2SO_4$	3.3	75.3	2.92	0.97	556	n.r	4.9	n.r	4.89
method 3 (Scheme 2.3)									
MACHT	7.49	54.1	5.02	5.45	<1	-	-	1.1	n.d
ACSHT	5.48	54.1	4.62		<1	-	-	n.d	n.d
HTCSO3H	n.d	n.d	n.d		15	0.012	1.3	n.d	n.d
FeCS	0.49	20.74	1.47	0.96	<1	-	-	n.d	n.d

The elemental composition and the textural properties of the catalysts are summarized in Table 3.2, and they clearly show the effects of starting biomass composition and preparation method on textural properties. Overall, the chemically activated sulfonated carbons (MACS, PACS, JACS, AC450S, AC500S, AC600S, CACS and $MACH_2SO_4$) were found to be a mixture of mesoporous and microporous particles with a high specific surface area of 93-690 $m^2g_{cat}^{-1}$, while the hydrothermally obtained sulfonated catalysts (MACHT, ACSHT and FeCS) were non-porous and exhibited a low specific surface area of 1-15 $m^2g_{cat}^{-1}$, similar to the non-activated carbons (1-10 m^2g^{-1}, data not shown). Also, the results indicate that under identical activation conditions, the porosity development was only affected by the properties of raw material and was disfavoured when the raw material contained a high amount of protein. Here, sulfonated carbons (also the non-

sulfonated forms) derived from biomass samples with low protein or N% (P and M cake) exhibited larger specific surface area, pore diameter and mesopore content than the J cake based materials (Table 3.2). Also, the higher specific surface area, pore volume and pore diameter observed for the non-sulfonated materials confirmed that sulfonation introduced bulky $–SO_3H$/$–PhSO_3H$ groups on catalyst surfaces. Interestingly, in case of sulfonated carbons obtained by method 2, the textural properties were almost similar to non-sulfonated forms suggestive of a less useful $–SO_3H$ incorporation, this difference could be partly attributed to the smaller size of $–SO_3H$ groups.

3.1.2. Thermal stability of catalyst

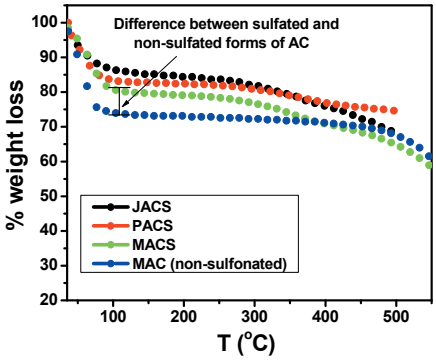

Figure 3.4. Representative TGA patterns of the sulfonated carbon materials obtained from DOWC, the non-sulfonated material is shown as a control.

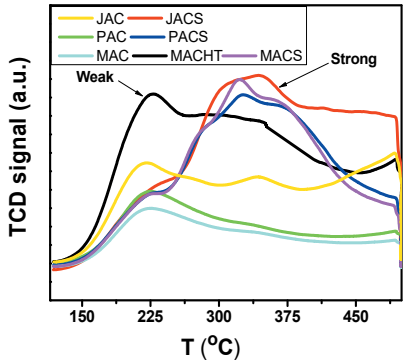

Figure 3.5. Typical NH_3-TPD profiles of catalytic materials obtained from DOCW under different conditions.

The novel carbon catalysts showed excellent thermal stability under oxygen-free conditions which is comparable to the previously reported sulfonated carbon catalysts.[17-19,23] Overall, the catalytic materials obtained by method 1 demonstrated high operational stability and were suitable for applications at operating temperatures (T_{max}) close to 240 °C (Table 3.3). The TGA patterns of sulfonated carbons show two distinctive weight loss regions (Figure 3.4): the first, more rapid loss occurred between 0-130 °C which was attributed to loss of water and free moisture adsorbed on the catalyst surface and the second weight loss region occurred at 240-380 °C; the 6-8% weight loss in this region was attributed to the removal of $–SO_3H$ groups, as this region was absent in the non-sulfonated materials. Following the 2nd region, weight loss continued but at a much slower rate which could be attributed to further the $–SO_3H$ loss with graphitization. To summarize,

sulfonation lowered the onset of thermal decomposition due to incorporation of $–SO_3H$ groups on carbon surface.[23] Further, the description of the influence of the raw material on the thermal stability of these materials can be found in the publication [**I**]. In contrast, the lower T_{max} values of the catalysts obtained by method 3 could be accredited to the partially carbonized and functionalized carbon structures produced by hydrothermal carbonization.

3.1.3. Acidic properties of catalysts

The acidic properties of the novel carbon catalysts were evaluated by temperature-programmed desorption of ammonia and titration methods. The results of the acidity measurements are summarized in Table 3.3. The acidities of the catalysts decrease in the following order:

(Sulfonated carbons) ACSHT >MACHT >AC600S >JACS > AC500S >PACS >MACS > AC450S>MAC-SO_3H >MACH_2SO_4 >CACS > FeCS > (non-sulfonated carbons) AC450 >AC500 >AC600 >CAC > (zeolites) H-ZSM-5 >H-Y >H-beta

Figure 3.5 shows the typical NH_3-TPD profiles of the novel carbon catalysts. For all sulfonated catalysts, two distinctive peaks were observed: a weak acid site around 210-230 °C and a strong acid site at 310–370 °C (the peak is not observed for non-sulfonated carbon). Here, the strong acid sites were ascribed to $–SO_3H$/$–PhSO_3H$ and phosphate groups, whereas weak acid sites were attributed to the surface functional groups (–OH, –COOH and lactones). It is important to note that in our experiments, we restricted the NH_3-desorption temperature to 500 °C, since sulfonation also reduces the thermal stability of carbonized materials and 500 °C was found to be the maximum temperature up to which most of the $–SO_3H$ remained attached to the catalyst surface, as also stated by Kastner *et al.*[23] Also, the trend based on NH_3-acidity was in good agreement with the titration results (higher acidity for more functionalized materials); but, it is also worth pointing out that NH_3-acidities were approximately ~30% higher than the acidities based on titration, which is in good agreement with trends found in literature. This overestimation could be most likely accredited to desorption of SO_x species along with NH_3 at temperatures 240-500 °C, due to removal of the sulfonic groups from the catalyst surface; indicating the limitations of NH_3-TPD method for acidity measurements of sulfonated carbon materials. Nonetheless, it is interesting to note that many authors have used NH_3 desorption temperatures up to 750-800 °C for acidity measurements of similar materials without taking into

account the stability of sulfonic groups leading to erroneous estimation of acidity.[24] Hence, the usefulness of the NH_3-TPD method for acidity measurements of sulfonic acid functionalized materials should be reviewed. The catalytic effects of sulfonated carbon materials have been credited to $–SO_3H$ groups, thus, their density has a distinct effect on the catalyst activity.[14-16] Herein, the presence of S and increased surface acid site densities of the sulfonated materials were consistent with the success of the sulfonation step (Table 3.3). The $–SO_3H$ acidities of the novel carbon catalysts decrease in the following order:

ACSHT >MACHT >AC600S >JACS >AC500S >PACS >MACS >MAC-SO_3H >CACS >FeCS > $MACH_2SO_4$

Table 3.3. Acidic properties and thermal stability of catalytic materials

Catalyst	[a]Total acid density	[b]NH_3 acidity	[c]-SO_3H density	T_{max}
	$mmolH^+g^{-1}$	$mmolg^{-1}$	$mmolg^{-1}$	°C
JAC	3.24	4.34		470
PAC	2.58	2.01		500
MAC	1.91	1.76		500
AC450		1.72		
AC500		1.17		
AC600		1.15		
CAC		1.1		
Post sulfonation materials				
method 1 (Scheme 2.1)				
JACS	3.96	6.2	0.7	240
PACS	3.62	5.86	0.84(0.83)	248
MACS	3.01	5.63	0.75	245
MAC-SO_3H	2.01	n.d	0.73	242
AC450S		4.68	0.68	n.d
AC500S		6.07	0.82	n.d
AC600S		6.36	0.91	n.d
CACS		5.12	0.53	n.d
ACSO3H	3.64	n.d	0.82	n.d
method 2 (Scheme 2.2)				
$MACH_2SO_4$	2.426	n.d	0.30*(0.13)	
method 3 (Scheme 2.3)				
MACHT	4.2	6.4	1.30*	210
ACSHT		6.84	1.13	204
HTCSO3H	4.24	n.d	1.13	205
FeCS		n.d	0.3	n.d

[a] determined by NaOH titration
[b] determined from NH_3-TPD curves
[c] based on CHNS analysis (represent values for spent catalyst after 3rd esterification cycle).
*SO_3H density =(SH+SO_3H)

The variations observed in $–SO_3H$ densities among these materials were in agreement with effects of raw material and preparation method on catalyst acidity. Comparison of the above trend and active carbon support properties in Table 3.2 revealed a clear relation between $–SO_3H$ density and C contents of active carbon prepared by method 1. The increased $–SO_3H$ density with increasing C content in active carbon could be caused by the functionalization of additional 4-BDS radicals resulting from availability of more aromatic carbon sheets (Sp2 sites, supported by XPS, Table 3.1 and 3.2) for $–PhSO_3H$ attachment. On the contrary, the H_2SO_4 treated active carbons ($MACH_2SO_4$) exhibited relatively low -SO_3H density, as it was difficult for H_2SO_4 to react with the rigid, aromatized and ordered carbon

frameworks even at elevated temperatures. Similarly, the high –SO_3H density in MACHT (method 3) could be originated from the easier sulfonation of the partially carbonized (less aromatic) structures formed under hydrothermal conditions and consistent with literature data which suggests that non-graphitic carbons (less aromatized ones) are easier to react with H_2SO_4 than aromatized graphitic carbons.[15] Nonetheless, successful sulfonation of the ordered carbon materials has been demonstrated with stronger sulfonating agents like fuming H_2SO_4, gaseous SO_3, ClH_3SO_4/H_2SO_4 mixture.[23,24] Consequently, the present study shows sulfonation by 4-BDS to be a more efficient method for sulfonating carbon materials with aromatized or graphitic structure (Sp2 carbons), contrary to the conventional sulfonation process (conc. H_2SO_4, SO_3) reported as a more efficient strategy for non-graphitic carbons. Accordingly, the combination of activation (chemical or physical) and radical sulfonation (method 1) may be a valuable technique for obtaining biomass-derived sulfonated carbon catalysts which possess high porosity and acidity simultaneously. Using the combination of the abovementioned steps we have been able to prepare mesoporous sulfonated carbon catalysts with pore volume ~0.46 cm^3g^{-1}, average pore diameter ~4.8 nm and –SO_3H density upto ~0.84 $mmolg^{-1}$. Furthermore, our results also showed that the amount of 4-BDS/sulfanilic acid had a negligible effect on catalyst –SO_3H density as the M DOWC based catalysts MACS (prepared at 15:1 w/w ratio of sulfonating agent to AC) and MAC-SO_3H (prepared by same method but with 4-BDS to AC w/w ratio of 2:1) exhibited comparable –SO_3H density (Table 3.3) but instead it depends on the amount of Sp2 C sites available (i.e. carbon content) for 4-BDS radical attachment.[19] In terms of weak acid sites, the sulfonated and non-sulfonated material exhibited similar –OH, –COOH density as the sulfonation process (in particular method 1) did not affect the weakly acidic groups. Although the sulfonation with H_2SO_4 (98%) caused oxidation of some of the AC sheets, its influence on overall material acidity was insignificant (Table 3.3).

3.1.4. Scanning electron microscopy and energy dispersive X-ray microelement mapping

SEM pictures also clearly show the distinctive effects of preparation method and starting material composition on the morphology of the novel carbon catalysts. A clear difference existed in the topography of the chemically activated and the non-activated materials. The non-activated carbons clearly exhibited a non-porous topography, while the appearance of large cracks and holes was consistent with the development of meso- and micropores in the phosphoric acid treated materials.

On the other hand, the effect of carbon source on porosity development could be clearly seen from the difference in topography of chemically activated J (flake like) and M (particle like) cakes (Figure 3.6).

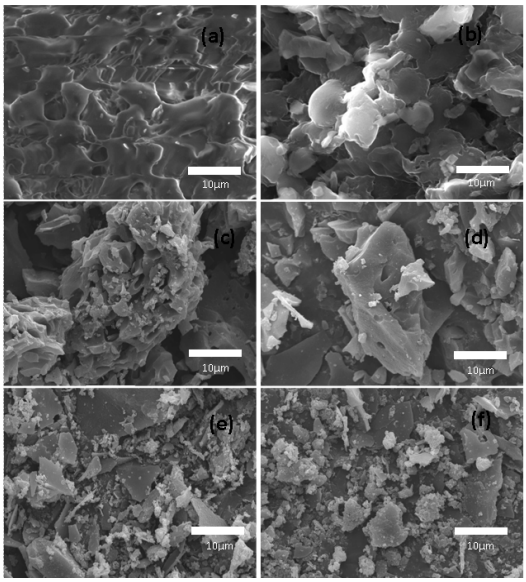

Figure 3.6. SEM images of selected carbon materials (a) MACHT (b) MAC* (unactivated) (c) MAC (d) MACS (e) JAC (f) JACS obtained from DOWC under different conditions.

SEM images also confirm that the carbon materials did not undergo any drastic morphological changes due to sulfonation. Additional details on the corresponding EDX element mapping (C, O and S) indicating homogeneous distribution of the different surface acid sites (-$PhSO_3H$, -OH and -COOH) in these materials could be found in publication **[I]**.

3.1.5. Transmission electron microscopy

TEM micrographs of the selected sulfonated carbon catalysts MACHT, MACS, PACS and JACS are shown in Figure 3.7. The TEM images clearly show the presence of a non-uniform carbon structure with randomly arranged aromatic carbon sheets in all the catalytic materials. Also, the morphology was distinctly different for the hydrothermal MACHT and the chemically activated sulfonated carbons MACS, PACS and JACS. The non-activated catalyst MACHT, closely resembled the corncob derived sulfonated carbons reported by Arancon *et al.*[25] The highly textured surface morphology and appearance of well-developed mesopores in the chemically activated sulfonated carbons were in good agreement with the results of N_2 physisorption (Table 3.2). The effect of raw material on porosity development was further clarified from the dissimilar morphology observed for MACS, PACS and JACS; a highly textured and coarse surface morphology with well-developed pores as large as ~11 nm observed for PACS and MACS were characteristics of a dominant mesoporous structure and were well reflected by their textural properties, whereas JACS with its slightly less coarse morphology exhibited features typical to less porous material (Figure 3.7).

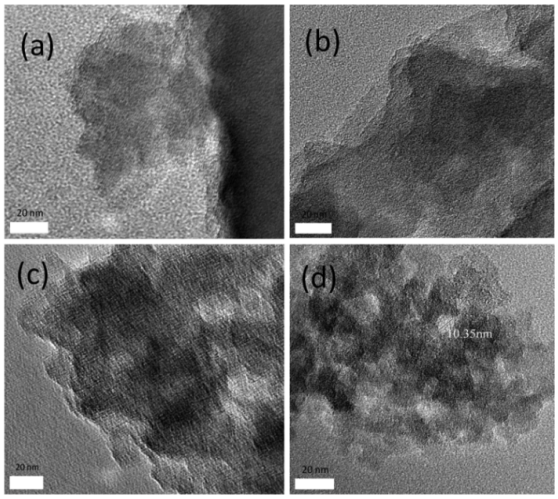

Figure 3.7. HR-TEM images of the sulfonated carbons: (a) MACHT (b) JACS (c) MACS and (d) PACS (scale bar 20 nm).

3.2. Catalyst activity results

3.2.1. Cellulose hydrolysis [I]

Hydrolysis of cellulose involves breaking of β-1,4-glycosidic bonds of the large polysaccharide units with H_2O, and produces the building monosaccharide (Scheme 3.1). It has been reported that over sulfonated materials hydrolysis takes place in two steps, the first step involving the breakdown of large polysaccharide units to water soluble oligomers (glucans) which are subsequently adsorbed on catalyst surface and hydrolyzed to sugars by the catalytic action of strongly acidic $–SO_3H$ groups/sites. Further, the weakly acidic –OH, -COOH groups/sites present in sulfonated carbon materials are reported to promote adsorption of these oligomers, thus, density of such groups can greatly influence the catalytic efficiency of sulfonated materials in cellulose saccharification.[15,16]

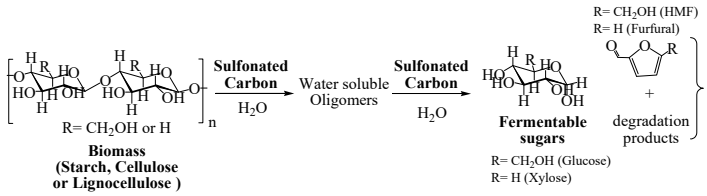

Scheme 3.1. Hydrolysis of cellulose/biomass.

The results obtained for the DOWC based novel carbon catalysts (Series I) are in good agreement with the above effects. Here, the negligible activities of un-sulfonated materials are in agreement with non-catalytic effects of the weakly acidic (-COOH, -OH) and the phosphate groups. Further, in terms of molar sugar (glucose) yield, the novel sulfonated catalysts not only outperformed H_2SO_4 (0.1 $molL^{-1}$), zeolites, ion-exchange resins and sulfated zirconia, but some of these catalysts also outperformed a number of sulfonated catalysts reported earlier works (Table 3.4) [**I**]. As in the studies before, the sugar yields were influenced mainly by $–SO_3H$ density, porosity (pore size, surface area) and the density of weakly acidic sites on catalyst surface (i.e.

$mmolH^{+}g_{cat}^{-1}$). Among the investigated catalysts, those obtained by method 1 (MACS, PACS and JACS), produced the highest sugar yield (35-53 mol-C%) from amorphous cellulose in 24 h.

Table 3.4. Conversion of cellulose, sugar yield and TOF over different catalysts

Catalyst	Conversion (%)	Yield mol-C%	[b]TOF h^{-1}	Ref.
Blank	10	0	0	This work [I]
JAC	10	8	0.0064	
PAC	10	6.6	0.0066	
MAC	10	6	0.008	
JACS	61	53	0.0344	
PACS	60	46	0.0335	
MACS	60	35	0.0301	
MACHT	43	27	0.0164	
$MACH_2SO_4$	52	30	0.0388	
[a]H_2SO_4	63	32	0.0079	
H-Y (12)	21	10	0.0316	
JACS	90[x]	78[x]	0.0503	
[a]H_2SO_4	61.8	32.7	-	Literature data, ref. details in [I]
AC-SO3H	42.8	40.5	-	
H-Beta (13)	22	5	-	
H-ZSM (45)	10	8	-	
Sulfated ZrO_2	38	18	-	
Amberlyst-15	33.7	25.5	-	
CMK-3-SO_3H	95	74.5	-	
Resin carbon-SO_3H	62	54	-	
CSAC-SO_3H	60	45	-	
Cell-Carbon- SO_3H	45	35	-	
MWCNT-SO_3H	50	27	-	
Si33C66-823-SO_3H	60.7	50.4	0.15	

[a](0.1 $molL^{-1}$), [b] TOF = moles of glucose formed per mole of acid site per hour. Reaction conditions: cellulose: catalyst (w/w ratio) = ~1, 1 mL H_2O per 0.01 g amorphous cellulose or [x]IL treated biomass (*Mesua ferrea* L. DOWC), t = 24 h, T = 150 °C.

In contrast, the materials obtained by H_2SO_4 treatment, MACHT and $MACH_2SO_4$ were relatively less active due to their limited pore space and low $–SO_3H$ (strong acid site) density respectively [**I**]. The superior activity of the former (MACS, PACS and JACS) are therefore attributed to the presence of larger pores, high surface area and suitable combination of the density of strong (0.70-0.84 $mmolg_{cat}^{-1}$) and weak surface (3.24-1.91 $mmolH^{+}g_{cat}^{-1}$) acid sites. Further, when microcrystalline cellulose was used as a substrate, the sugar yield reduced by half, which may be attributed to the difficulties associated with getting through the highly packed and crystalline structure of untreated cellulose (crystallinity index ~82%) **[I]**. Typically, previous studies have employed amorphous cellulose obtained by ball-milling (48-72 h) as a substrate which is much easier to be hydrolyzed.[15,16,21] In contrast, here we have applied a more practical ionic liquid (IL) pretreatment with 1-ethyl-3-methylimidazolium chloride to reduce cellulose crystallinity. Compared to ball-milling, IL pretreatment has several advantages: short pre-treatment times (1-3 h), IL reuse and the possibility to dissolve and immediately regenerate large quantities of cellulose to its initial purity. IL selection was motivated by the efficiency of $Cl^{–}$ containing imidazolium ILs in cellulose dissolution resulting from their high hydrogen bond basicity as well as the low cost of this particular IL.[26]

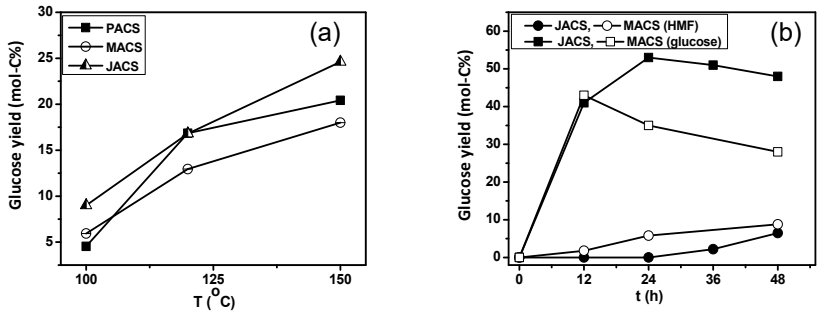

Figure 3.8. Glucose yield over the optimum DOWC biomass derived sulfonated carbon catalyst as function of (a) reaction temperature (investigated with microcrystalline or untreated cellulose substrate) and (b) reaction time (investigated with amorphous cellulose at 150 °C).

The highest sugar yield (74.5%, ball-milled cellulose substrate) reported for a solid acid catalyzed process is with CMK-3-SO_3H, an ordered mesoporous sulfonated carbon catalyst involving multi step synthesis.[27] Although the materials reported here did not outperform the CMK-3 catalyst, the 46-53 mol-C% yield obtained for P and J cake based materials were on a very high side, especially considering their easy preparation, superiority over many other sulfonated catalysts, glucose selectivity and, in particular, the ability to directly convert lignocellulosic biomass (90 % conversion) with high sugar selectivity (total sugar yield of 78%) (Table3.4). Besides, sugar yield can further be improved with optimization of reaction parameters, pretreatment conditions etc. Herein, the inferior saccharification activity of M cake based catalyst, MACS was obtained due to formation of degradation products which was favored by inadequate adsorption of glucans due to slightly smaller pores, lack of weakly acidic sites and the high –SO_3H density (Figure 3.8). Further investigation with respect to reaction temperature showed 150 °C to be the optimum reaction temperature as degradation of glucose to 5-HMF and levulinic acid became prominent at higher reaction temperatures, while typical reaction time of 12-24 h was required to attain maximum glucose yield (Figure 3.8(b)). However, when reusability studies were performed with the spent JACS, glucose yield increased from 51 to 61 mol-C%, which is most likely due to inclusion of the unreacted cellulose particles of the previous experiment in the reactor. In addition, it was difficult to fully separate the spent catalyst and unreacted cellulose particles, causing glucose overestimation in the successive run.

3.2.2. Oleic acid esterification [I]

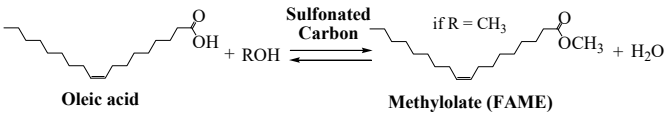

Scheme 3.2. Reaction scheme for esterification of oleic acids with methanol.

To investigate the prospective of the DOWC derived materials as biodiesel catalysts, oleic acid (OA) esterification was used as a model reaction (Scheme 3.2). In contrast to cellulose saccharification, esterification is a more straightforward and less energy intensive process. Nonetheless, it involves large fatty acid molecules with typical kinetic diameter in the order of 2-2.4 nm. Thus, catalysts with large mesopores and high specific surface area are expected to be more efficient in converting molecules like OA. Besides, esterification is a highly reversible equilibrium reaction requiring use of catalyst, excess of alcohol and/or continuous H_2O removal to get high ester yields.

Figure 3.9 shows a summary of the esterification activity of the selected novel carbon catalysts in comparison to H_2SO_4 and selected zeolites. The results clearly illustrate the catalytic superiority of the sulfonated materials in comparison to H_2SO_4, zeolites, non-sulfated materials, and also point out the occurrence of a clear relation between catalyst structure (porosity, pore size, specific surface area etc.) and $–SO_3H$ density with ester yield, as also reported for similar biochar based sulfonated carbons in the literature.[23,24] Here, the negligible conversion levels achieved with non-sulfated materials were consistent with the non-catalytic effects of weakly acidic –COOH, –OH and phosphate groups. As expected, the highest acid conversions were obtained with the most porous PACS and MACS with relatively high $–SO_3H$ density of 0.75-0.84 $mmolg_{cat}^{-1}$ followed by the slightly less porous and acidic JACS ($–SO_3H$ density of 0.70 $mmolg_{cat}^{-1}$). On the other hand, the lower conversion obtained for MACHT could be attributed to its non-porous structure limiting accessibility of large OA (Table 1.1) substrate to the active sites. While, the even lower conversion recorded for the concentrated H_2SO_4 treated sulfonated catalyst, $MACH_2SO_4$ was attributed to its very low active site ($–SO_3H$) density (Table 3.3). Here, the insignificant catalytic effects of zeolites upon OA esterification is attributed to the limiting effects of pore space, surface acid site density as well as the lack of strong enough acid sites. Although increasing the methanol concentration observably increased conversion level for the less active JACS, $MACH_2SO_4$ and MACHT, yet it did not approach the levels achieved by MACS or PACS, Figure 3.9(b). Overall, the order of

esterification activity of the sulfated catalysts based on OA conversion was PACS=MACS >JACS >MACHT >H_2SO_4 >$MACH_2SO_4$, following a combined effect of acidity and porosity. The effects of alcohol chain length on conversion were also studied by repeating similar experiments with ethanol and 1-propanol with MACS as a reference catalyst. The conversion achieved with ethanol was only 80% and it reduced even further to 62% with 1-propanol, Figure 3.9(c), and in accordance with the reactivities of alcohols of different carbon chain lengths. Further, in terms of stability, the catalysts obtained by the method 1 also outperformed those obtained by the method 2 and 3. The poor reusability in the latter were accounted with the easy leaching of –SO_3H groups compared to the catalyst obtained by the method 1 (Fig. 3.9(d), Table 3.3), Yu *et al*.[24] reported a similar effect in sulfonated activated biochar catalysts obtained by H_2SO_4 treatment.

Table 3.5. Comparison of the esterification activity of the DOWC based novel sulfonated carbons with previously reported sulfonated carbon catalysts

Catalyst	**Raw material** (Carbon source)	**Sulfonating agent**	**T** (°C)	**Methanol/oil** (mole ratio)	**TOF** (h^{-1})	**TOF** (min^{-1})	Ref.
JACS	J DOWC	4-BDS	64	20	70.81	1.18	This work **[I]**
PACS	P DOWC	4-BDS	64	20	104	1.733	
MACS	M DOWC	4-BDS	64	20	102.3	1.705	
MAC-SO_3H	M DOWC	4-BDS	80	21	51.5	0.854	
MACHT	M DOWC	H_2SO_4	64	20	29.2	0.486	
$MACH_2SO_4$	M DOWC	H_2SO_4	64	20	26	0.433	
AgForm-400C-SO_4	biochar	H_2SO_4	47	20	-	0.04	Literature data, ref. details in **[I]**
PHC-400C-SO_4	peanut hull char	H_2SO_4	57	20	-	0.15	
WVB-20-SO_4	wood AC	H_2SO_4	57	20	-	0.18	
BX-7540-SO_4	wood AC	H_2SO_4	60	20	-	0.56	
WVB-20-SO_3	wood AC	SO_3	60	20	-	0.18	
SC-CCA3	resorcinol resin, γ-Al_2O_3	4-BDS	65	57	102	-	
Starbons-300A2	Starbon-300	$ClSO_3H/H_2SO_4$	80	10	509*	-	
S-AC	mesoporous AC	4-BDS	65	57	44	-	
Amberlyst-15	-	-	65	57	15	-	

*activity/mmol-SO_3H

To further fortify the viability of these biodiesel waste derived materials as catalysts in biodiesel production, the TOF values were compared to those previously reported for sulfonated catalysts (Table 5). As expected, the TOF of the optimal material, the radically sulfonated AC (PACS and MACS) catalysts were higher than those achieved with the hydrothermal and directly sulfonated AC (method 2 and 3) as well as the ones with sulfonated activated biochar, sulfonated AC (commercial), sulfonated OMCs and Amberlyst™-15 demonstrating their catalytic superiority. The results are in good agreement with the effects of catalyst –SO_3H density and porosity (Table 3.5).

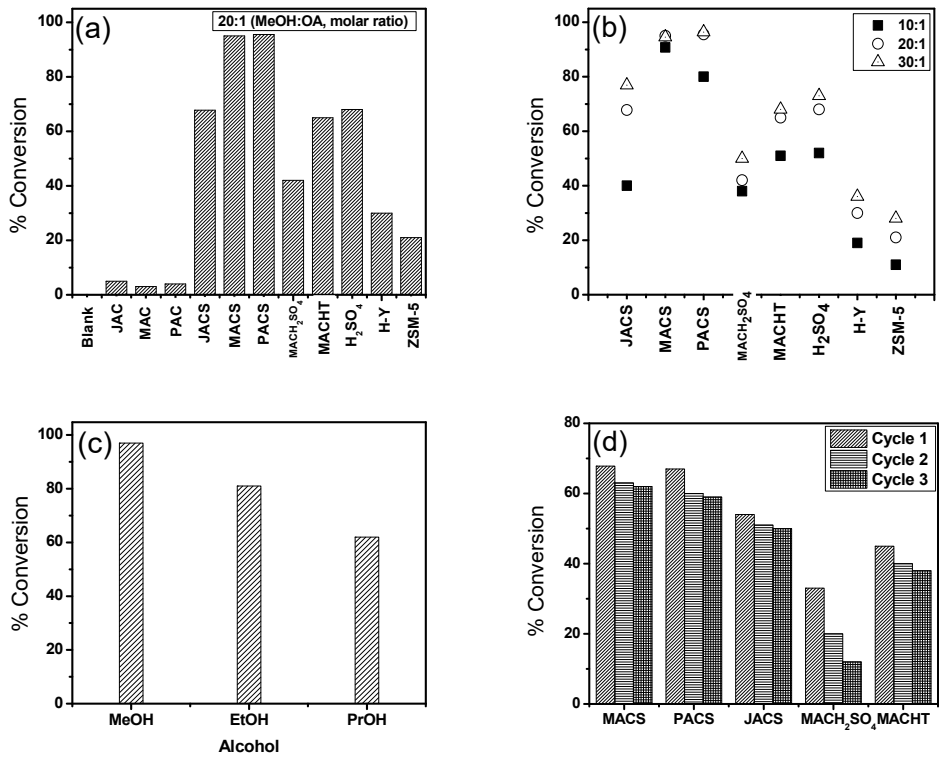

Figure 3.9. Esterification activity of the DOWC biomass derived catalytic materials (a) comparison with 98% H_2SO_4, zeolites and the non-sulfated forms (investigated at 20:1) (b) effect of methanol to oleic acid molar ratio (c) alcohol chain length (shown for MACS at 30:1) and (d) reusability (3 h reaction). Reaction conditions: catalyst loading = 3 wt% of acid or 0.02 g H_2SO_4 (equivalent to $–SO_3H$ in MACS), t = 10 h and T = 64°C.

However, the TOF of sulfonated starbon-300 was even higher (~5 times the best DOWC catalyst) which could be attributed to the presence of extremely large mesopores (average pore diameter >14 nm) and high $–SO_3H$ density. In contrast, the DOWC based catalysts reported here possessed a mixed texture with an average pore diameter of 3.9-4.9 nm; thus, the possibility of steric effect due to agglomeration of OA molecules at pore mouth was higher in the DOWC based catalysts compared to the sulfonated starbon-300 catalyst with very large pores. Overall esterification activities of the mesoporous DOWC catalyst obtained by the method 1 were higher than those achieved with ion exchange resins (Amberlyst-15) and the sulfonated biochars, commercial AC, OMCs and carbohydrate, respectively.

3.2.3. Simultaneous esterification and transesterification of vegetable oil [II]

Based on the promising catalytic activity of the novel carbon catalysts upon biodiesel production, the most active catalyst (PACS) from the above discussion was further selected for studying the reaction kinetics of simultaneous esterification and transesterification of acidic oils to biodiesel in a batch type reactor system. It was demonstrated that in our experiments that, in the presence of a mesoporous novel carbon catalyst, the reaction steps were kinetically controlled and not limited by inter-particle diffusion or external mass transfer limitations (preliminary experiments showed that the catalyst particle size and stirring speed have negligible effect on the rate of oil conversion). Accordingly, a simplified second order pseudo-homogeneous kinetic model was proposed omitting intra particle diffusion effects. The reaction steps involved in simultaneous esterification and transesterification of fatty acid containing acid oils were assumed to be a combination of all the equilibrium reactions separately involved in esterification and transesterification, with all forward and reverse reactions following the second-order kinetics in liquid phase (Scheme 3.3) [**II**].

FFA + MET $\Leftrightarrow$ W + FAME (3.1)
TG + MET $\Leftrightarrow$ DG + FAME (3.2)
DG + MET $\Leftrightarrow$ MG + FAME (3.3)
MG + MET $\Leftrightarrow$ GLY + FAME (3.4)

where,
FFA= Free fatty acid, MET = Methanol, W = H_2O,
TG = triglycerides, DG = diglycerides, MG = monoglycerides, FAME = fatty acid methyl ester

Scheme 3.3. The proposed reaction scheme for acid-catalyzed simultaneous esterification and transesterification of acidic oils.

Thus, assuming kinetic control, fatty acids of different lengths to react at the same rate and the rates of the non-catalyzed reactions to be negligible the reaction rate equations for a constant-volume isothermal batch reactor are:

$$r_1 = k_1\left(c_{FFA}c_{MET} - \frac{c_W c_{FAME}}{K_{eq1}}\right) \quad (3.5)$$

$$r_2 = k_2\left(c_{TG}c_{MET} - \frac{c_{DG}c_{FAME}}{K_{eq2}}\right) \quad (3.6)$$

$$r_3 = k_3\left(c_{DG}c_{MET} - \frac{c_{MG}c_{FAME}}{K_{eq3}}\right) \quad (3.7)$$

$$r_4 = k_4\left(c_{MG}c_{MET} - \frac{c_{GLY}c_{FAME}}{K_{eq4}}\right) \quad (3.8)$$

where, C_{FFA}, C_{MET}, C_W, C_{FAME}, C_{MG}, C_{DG}, C_{TG} and C_{GLY} denote the concentrations of FFA, methanol, water, FAME, MG, DG, TG and GLY, respectively. The rate constants given by k_1, k_2, k_3, k_4 and K_{eq1}, K_{eq2}, K_{eq3}, K_{eq4} represent the equilibrium constants for reactions (1), (2), (3) and (4), respectively. Here, the reactor model equation for each of the component 'i' in the batch reactor is given by $\frac{dc_i}{dt} = rho_B \times r_i$, where, $rho_B = \frac{M_{Cat}}{V_l}$ and it accounts for the loss of catalyst (M_{cat}) and the reduction of liquid phase volume (V_l) due to sampling. The temperature dependence of the rate constants (k_1, k_2, k_3, k_4) is accounted for with the Arrhenius equation as follows:

$$k_1 = k_{01} e^{-\frac{Ea_1}{R}\left(\frac{1}{T}-\frac{1}{\bar{T}}\right)} \quad (3.9)$$

$$k_2 = k_{02} e^{-\frac{Ea_2}{R}\left(\frac{1}{T}-\frac{1}{\bar{T}}\right)} \quad (3.10)$$

$$k_3 = k_{03} e^{-\frac{Ea_3}{R}\left(\frac{1}{T}-\frac{1}{\bar{T}}\right)} \quad (3.11)$$

$$k_4 = k_{04} e^{-\frac{Ea_4}{R}\left(\frac{1}{T}-\frac{1}{\bar{T}}\right)} \quad (3.12)$$

where, k_{01}, k_{02}, k_{03}, k_{04} are the frequency factors, E_{a1}, E_{a2}, E_{a3}, E_{a4} represent the activation energies, whereas $\bar{T}$ represents the mean temperature value from the experiments and R is the gas constant. The kinetic parameters were determined by non-linear regression analysis. The regression software 'MODEST' was used in all computations. The discrepancy of the fit model was checked by standard statistical analysis, and the 'kinetic model' was found to be ≥98 % accurate in explaining the experimental findings for three different feedstock oils with varying amounts of free fatty acid, monoglyceride, diglyceride and triglyceride (Figure 3.10). The rate constants (k), activation energies (E_a) and equilibrium constants (K_{eq}) of the individual reactions determined from the fit models for three different feedstock oils (Table 3.6 and 3.7) which confirmed the reaction steps to be kinetically controlled (E_a>25 kJmol^{-1} in all steps).

Furthermore, in addition to reaction temperature and methanol amount affecting kinetic parameters, the composition feedstock was also found to have distinct effects on the solubility of methanol and oil phase which influenced k, K_{eq} and E_a values and eventually determined the equilibrium/final biodiesel (FAME) yield. The detailed effects of these parameters on reaction kinetics and product yield have been individually discussed in publication **[III]**. The best results obtained in this work correspond to product (biodiesel) with FAME content between 79-91 wt% (120 °C and 20:1 methanol-to-FFA molar ratio) in a one step process; though, this does not confer

to EN14214 recommended 96.5 wt% FAME, the >90 FAME content obtained in this work is one of the highest values reported for a one step process.

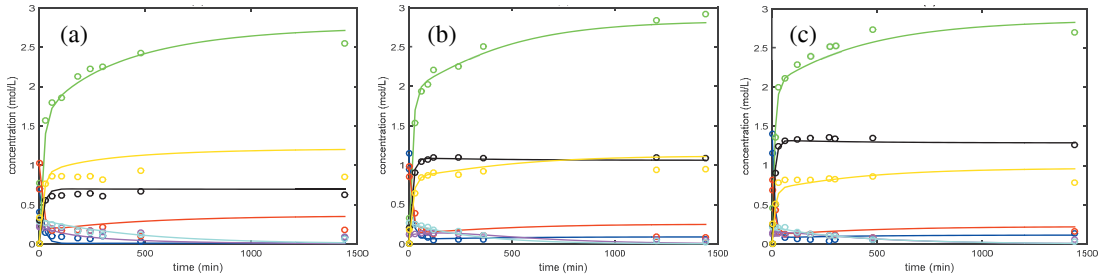

Figure 3.10. Kinetic plots of simultaneous esterification and transesterification of feedstock oil (a) I, (b) II and (c) III at 120°C. Reaction conditions: catalyst amount = 0.5 g and methanol to FFA in oil molar ratio = 20/1.Symbols: blue = FFA, green = FAME, red = MG, magenta = TG, cyan = DG, black=Water, yellow=GLY, solid lines-model, circles-experimental point.

Most importantly, to account for the loss of activity of sulfonated catalysts upon reuse, a simple deactivation model based on the '*time-on-stream'* theory of catalyst decay was proposed. Here, the catalyst deactivation was accounted for in terms of concentration-independent deactivation constant (k_d) which could describe another parameter (r_d). In the deactivation model, activation energies were taken from kinetic model data of the fresh catalyst with one of the feedstock and the reaction rates (r_i) were simply multiplied by the term (r_d). The relevant parameters (k_1-k_4, k_{01}-k_{04} and K_{eq1}-K_{eq4}) estimated from fit models at 4th reaction cycle are presented in Table 3.8.

$$r_d = e^{(-k_d \times (t + t_{TOS}))} \qquad (3.13)$$

Here, the parameter r_d is a measure of fraction of active sites and ($t + t_{TOS}$ =reaction time of previous run + time-on-stream). Comparison of the reaction rate constants (k values) in Table 3.6 and Table 3.7 show the reduction in k_1 and k_4 of the order (2.1 and 2 times) while k_2 and k_3 to be by 1 and 1.5 times, respectively. Overall, the proposed deactivation model could account for the loss of catalyst activity (due to active site blocking) with 94 % confidence. Also, the reduced K_{eq2}-K_{eq4} value was consistent with shifting of reaction equilibrium in backward direction which was consequently reflected by a reduced formation of FAME. Even so, the final FAME yields could still reach ~62 wt% and it could be supposed that with respect to FAME yield the catalytic material retained 75% of its original activity for simultaneous esterification and transesterification, a major improvement when compared to solid acid catalysts reported in earlier works **[II].**

Table 3.6. Rate constants of forward reactions estimated by regression analysis

Feedstock (Methanol/FFA- mole ratio)	**T** (° C)	**k_1** $Lmol^{-1}min^{-1}$	**k_2** $Lmol^{-1}min^{-1}$	**k_3** $Lmol^{-1}mol^{-1}$	**k_4** $Lmol^{-1}min^{-1}$
Oil I (40/1)	80	1.68×10^{-2}	6.60×10^{-4}	5.90×10^{-4}	1.27×10^{-2}
Oil I (40/1)	100	5.66×10^{-2}	2.29×10^{-3}	4.32×10^{-3}	4.69×10^{-2}
Oil I (40/1)	120	1.68×10^{-1}	6.90×10^{-3}	2.58×10^{-2}	1.52×10^{-1}
Oil I (20/1)	120	1.29×10^{-1}	4.98×10^{-3}	1.18×10^{-2}	1.38×10^{-1}
Oil I (10/1)	120	1.12×10^{-1}	4.10×10^{-3}	9.57×10^{-3}	1.08×10^{-1}
Oil II (20/1)	80	1.41×10^{-2}	6.60×10^{-4}	4.90×10^{-4}	1.17×10^{-2}
Oil II (20/1)	100	4.33×10^{-2}	2.12×10^{-3}	2.06×10^{-3}	3.40×10^{-2}
Oil II (20/1)	120	1.19×10^{-1}	6.08×10^{-3}	7.43×10^{-3}	8.88×10^{-2}
Oil III (20/1)	80	1.59×10^{-2}	1.10×10^{-3}	1.08×10^{-3}	1.88×10^{-2}
Oil III (20/1)	100	4.64×10^{-2}	2.76×10^{-3}	2.84×10^{-3}	4.40×10^{-2}
Oil III (20/1)	120	1.22×10^{-1}	6.30×10^{-3}	6.79×10^{-3}	9.44×10^{-2}

Table 3.7. Activation energies (E_a) and equilibrium constants (K_{eq}) estimated by parameter fitting of the kinetic model

Feedstock	**E_{a1}** $kJmol^{-1}$	**E_{a2}** $kJmol^{-1}$	**E_{a3}** $kJmol^{-1}$	**E_{a4}** $kJmol^{-1}$	**K_{eq1}**	**K_{eq2}**	**K_{eq3}**	**K_{eq4}**
Oil I	66.40	67.90	109.00	71.50	1.42×10^{1}	8.82×10^{7}	4.95×10^{7}	8.16×10^{-1}
Oil II	61.40	64.20	78.20	58.50	1.66	3.34×10^{7}	8.31×10^{6}	6.23×10^{-1}
Oil III	58.70	50.30	53.10	46.50	1.26	2.13×10^{-1}	5.18×10^{5}	4.90×10^{-1}

The K_{eq} values are reported for mean reaction temperature (100 °C)

Table 3.8. The rate constants (k), the equilibrium constants (K_{eq}) and the deactivation factor (k_d)estimated by parameter fitting of the catalyst deactivation model

k_1 $Lmol^{-1}min^{-1}$	**k_2** $Lmol^{-1}min^{-1}$	**k_3** $Lmol^{-1}mol^{-1}$	**k_4** $Lmol^{-1}min^{-1}$	**K_{eq1}**	**K_{eq2}**	**K_{eq3}**	**K_{eq4}**	**k_d**
2.65×10^{-2}	3.06×10^{-3}	2.89×10^{-3}	2.29×10^{-2}	1.75	6.87×10^{5}	1.21×10^{6}	3.76×10^{-1}	5.58×10^{-4}

The k, K_{eq} and k_d values are reported for mean reaction temperature (100 °C)

3.2.4. Glycerol acetylation [III]

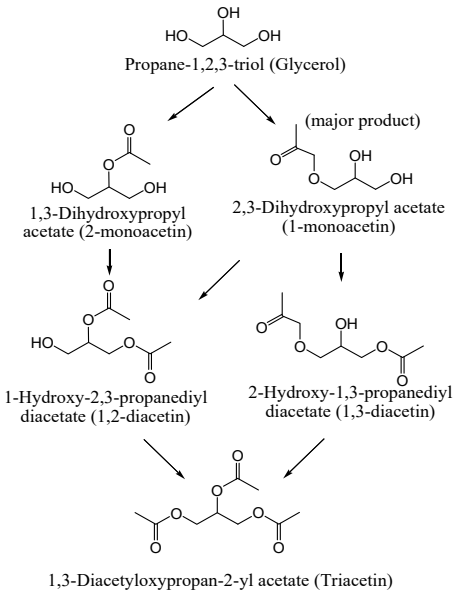

Scheme 3.4. Reaction scheme for acetylation of glycerol to triacetin

In view of the importance of the conversion of surplus glycerol from biodiesel production to high value derivatives, the catalytic potential of the novel carbon catalysts (Series II) was investigated in the acetylation of glycerol to triacetin with acetic anhydride (Scheme 3.4). Triacetin is a high value glycerol derivative with applications in food, pharmaceuticals, cosmetics and as a oxygenate fuel additive for diesel and biodiesel.[6,8] Unlike acetylation with acetic acid, acetylation of glycerol with acetic anhydride is an exothermic reaction and proceeds smoothly even in the absence of a catalyst. Nonetheless, it has been established that the formation of di- and triacetin involving successive acetylations of the second and third hydroxyl groups of glycerol is affected by the catalyst acidic properties.[6,8] Thus, the aim of this study was to study the influence of reaction parameters, catalyst structure (pore structure and size) and acidic properties on triacetin formation on the basis of experiments conducted over a range solid acids with varying structure and acidic properties (H-Y, H-beta, H-ZSM, novel carbons series II: AC450, AC500, AC600, AC450S, AC500S, AC600S and ACSHT, Table 3.2 and 3.3) in catalytic amounts. To clarify the effect of catalyst structures on triacetin formation/product selectivity, the dimensions (critical diameter, length, surface area and volume) of reactants and products molecules were determined by DFT calculations (Figure 3.11), co-related with the molecular dimensions and the properties of the catalysts (pore volume, pore size, specific surface area). The significance of the study was that 100% triacetin selectivity could be achieved in glycerol acetylation with acetic anhydride in 20-50 min in the presence of catalytic amounts of mesoporous sulfonated carbons (AC450S, AC500S and AC600S) and zeolite H-Y. Our results confirmed that the selectivity to triacetin was influenced mainly by the pore structure and catalyst surface acid site density and for the contribution of each of the factor was different among the two classes of catalysts: microporous (zeolites) and mesoporous (carbons) (Table 3.9).

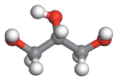

Propane-1,2,3-triol
(Glycerol)
d_c = 6.46 Å
l = 3.85 Å

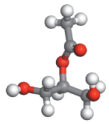

1,3-Dihydroxypropyl acetate
(2-Monoacetin)
d_c = 5.92 Å
l = 5.14 Å

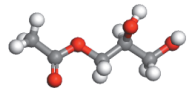

1,3-Dihydroxypropyl acetate
(1-Monoacetin)
d_c = 8.59 Å
l = 3.09 Å

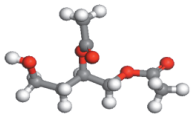

1-Hydroxy-2,3-propyldienyl
diacetate (1,2-Diacetin)
d_c = 7.80
l = 3.85 Å

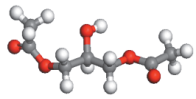

2-Hydroxy-1,3-propyldienyl
diacetate (1,3-Diacetin)
d_c = 9.43 Å
l = 3.12 Å

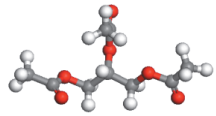

1,3-Diacetyloxypropan-2-yl
acetate (Triacetin)
d_c = 10.206 Å
l = 3.85 Å

Figure 3.11. The DFT-optimized structures of glycerol and the product molecules formed during acetylation. The grey, red and white balls represent C, O and H atoms, respectively. Here, 'dc'is the critical diameter and 'l' is length of the molecule.

The shape selectivity effect was dominant in microporous zeolites and was verified from the molecular dimensions of glycerol, monoacetin, diacetin and triacetin obtained from DFT calculations; on the contrary, in mesoporous catalysts surface acid site density was found be the main factor responsible for determining triacetin selectivity **[III]**. Further, upon reuse the best catalysts, sulfonated carbons (AC500S) and zeolite H-Y, however, showed a slight loss of activity which was more severe for H-Y and 100% triacetin selectivity could not be maintained as adsorption of the reactants in pores might have easily caused reduction in the available pore space (I_s), thus, preventing the formation of triacetin. Loss of active sites may have also contributed to this effect. In contrast for mesoporous AC500S triacetin selectivity, although slightly reduced upon reuse (most likely due to pore blockage), but it was still possible to obtain ~100% selectivity by simple extension of reaction time **[III]**.

Table 3.9. Influence of catalyst on product selectivity

Catalyst	Selectivity at 50 mol % Conversion			Selectivity at 90 mol % Conversion			Selectivity at 100 mol % Conversion		
	mono-	di-	tri-	mono-	di-	tri-	mono-	di-	tri-
H-ZSM-5	100	0	0	83.1[c]	16.9[c]	0[c]	0[d]	40.6[d]	59.4[d]
H-beta	n.a	n.a	n.a	39	34	27	0[d]	34.3[d]	65.7[d]
H-Y	n.a	n.a	n.a	0	0	100	0[e],0[d]	0.2[e],0[d]	99.8[e],100[d]
ACSHT	n.a	n.a	n.a	n.a	n.a	n.a	0[d]	45[d]	65[d]
MCM-41	89.6[b]	10.4[b]	0[b]	82	13.8	4.2	75.5[d]	16.2[d]	8.16[d]
MCM-48	75.7[b]	24.3[b]	0[b]	75.2	17	7.8	46[d]	43.6[d]	10.4[d]
MCM-48[a]	n.a	n.a	n.a	n.a	n.a	n.a	40[d]	47.3[d]	12.7[d]
AC450	47.4	52.6	0	53.4	46.6	0	50.9[d],0[f]	48.4[d],62.1[f]	0.7[d],37.9[f]
AC500[a]	44.7	55	0	55.3	44.4	0	55[d],2.5[f]	43.8[d],58.7[f]	1.2[d],38.8[f]
AC600	55	42.8	2.2	54.8	45.2	0	53.4[d],2.6[f]	46.6[d],61.9[f]	0[d],35.5[f]
AC450S	n.a	n.a	n.a	0	12	88	0[d]	0[d]	100[d]
AC500S	n.a	n.a	n.a	0	23.8	76.2	0[e],0[d]	10[e],2[d]	91[e],98[d]
AC500S[a]	0	47	63	0	31	69	0[d]	18.8[d]	81.2[d]
AC600S	0	27	73	0	10	90	0[d]	0[d]	100[d]
Blank	72.3	27.7	0	65[c]	34[c]	1[c]	4.3[e]	61[e]	34.7[e]

Reaction conditions: catalyst = 0.25 g (~5 wt% of glycerol) or [a] equivalent to 0.3 mmol of H^+, T = 100 °C, Ac_2O:glycerol (molar ratio) = 5, no stirring; n.a=data not available.
[b] Represent selectivity at 60±3 mol-% conversion,
[c] Represent selectivity at 80±3 mol-% conversion,
[d] 50±5 min reaction time, [e]20 min reaction time,
[f] 120 min reaction time (represents maximum observed triacetin selectivity),
[e]180 min reaction time (represents maximum observed triacetin selectivity).

Also, to explain our experimental findings, new reaction pathways were proposed (Scheme 3.5 and 3.6) for the two different catalyst groups (mesoporous and microporous). Mechanistically, glycerol acetylation takes place in four steps and proceeds through either the catalyst stabilized $A_{AC}1$ or $A_{AC}2$ mechanism.[28]In microporous zeolites, the $A_{AC}1$ type mechanism prevails (Scheme 3.5) as the formation of a tetrahedral intermediate is sterically unfavorable inside the microporous materials due to steric constraints.[29]Here, the possibility of multiple (simultaneous) acetylation steps to occur is ruled out as the surface acid site densities of zeolites are naturally very low. On the contrary, in case of mesoporous materials (MCM-41, MCM-48 and the mesoporous carbon catalysts), it was proposed that the reaction predominantly proceeds through a type of pathway involving tetrahedral $A_{AC}2$ since the formation of a tetrahedral intermediate requires less energy and its formation is also sterically not hindered due to large pores of the catalyst (Scheme 3.6).

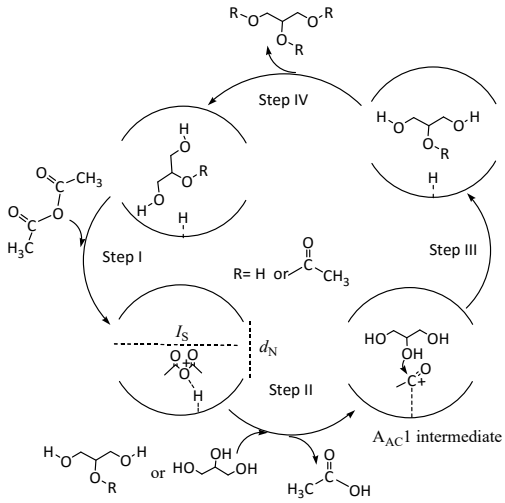

Scheme 3.5. Plausible reaction mechanism for acetylation of glycerol with acetic anhydride in the presence of microporous zeolite catalysts ($A_{AC}1$ pathway).

Also, it is likely that direct acetylation of glycerol to triacetin takes place as in these large pore materials as the product selectivity is not limited by any steric constrains and the reaction Gibbs free energy corresponding to direct acetylation of glycerol to triacetin is the lowest (-122.23 kJmol^{-1}) **[III]**. Meanwhile, with acetic acid, the maximum triacetin selectivity was rather poor (0% and 9% for H-Y and AC500S, respectively). Finally, the selectivity can be tuned to favor any one of the products (mono-, di- or triacetin) provided the right combination of a catalyst and reaction conditions are chosen.

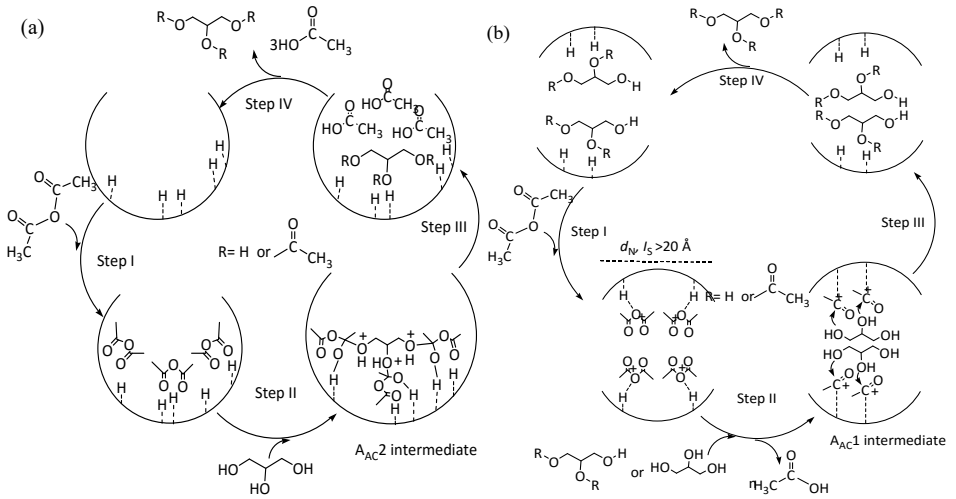

Scheme 3.6. Plausible reaction mechanism for acetylation of glycerol with acetic anhydride in the presence of mesoporous catalysts (a) $A_{AC}2$ pathway and (b) $A_{AC}1$ pathway.

3.2.5. Fatty acid (lauric, oleic) esterification with glycerol [IV]

The catalytic potential of the novel sulfonated carbons (selected) were also investigated for monolaurin (a commercially important surfactant) production by liquid phase esterification of equimolar mixtures of glycerol and lauric acid (Scheme 3.2, fatty acid = lauric acid and R = $–CH_2CH(OH)CH_2(OH)$). Two different sulfonated catalysts (with different pore structures and surface acidities, viz. ACSO3H and HTCSO3H, Tables 3.2 and 3.3) were applied to investigate the effects of catalyst properties on monolaurin selectivity and yield. Protonated zeolites (medium pore H-Y and small pore H-ZSM-5), H_2SO_4 and active carbon were used as reference catalysts for the sake of comparison. In agreement with the trends found in the literature, our results also demonstrated the existence of strong shape selectivity effect imposed to the reaction products by size limitations imposed by the catalyst pore apertures. The initial rates of fatty acid conversion calculated per time unit decreased in the following order: ACSO3H> H_2SO_4> HTCSO3H> H-Y> H-ZSM-5, which is also correlating with the catalyst acid site density, pore size and dimensions of reacting molecule. However, HTCSO3H and H-ZSM-5 were exceptions in this regard and exhibited unpredictably high catalytic activity (initial rate, conversion and monolaurin selectivity).

Table 3.10. Initial rate, turnover frequency (TOF), the ratio between the initial rate of formation of MG to DG, conversion of lauric acid at 10 h*mmolH^+ normalized yield and selectivity to MG at 40 mol-% conversion of lauric acid.

Catalyst	**Initial rate** (mmol min^{-1})	**TOF** (mmol min^{-1})	[a] r_{MG}	[b] **Conversion** (mol-%)	**Selectivity to MG at 40 mol-% conversion**
ACSO3H	6.13	747.19	2.3	50	72
HTCSO3H	1.6	155.75	2.4	17	n.a
HY	0.53	64.39	1.7	30	73
H-ZSM-5	0.42	34.66	1.46	20	77
H_2SO_4	4	243.90	1.2	n.a	45

[a] r_{MG} =Initial rate of MG formation /Initial rate of DG formation

[b] acid conversion at normalized time of 10 h*mmol H^+

Conditions: 125 °C, 0.5 g catalyst.

It should, however, be stated that HTCSO3H presented a high density of hydrophilic acid sites while H-ZSM-5 presented a high specific surface area (443 $m^2g_{cat}^{-1}$) and moderate acid site concentration, thus, facilitating proper dispersion of acidic sites and this availability of active sites for adsorption of reactants even on external surface was in turn reflected in terms of the high initial rates. A better representation of the catalyst activity was given by the TOFs, where upon the following trend was observed: ACSO3H>> H_2SO_4> HTCSO3H > H-Y > H-ZSM-5 which directly correlated with the combined effects of catalyst acid site density and pore dimensions. Further, the ratio between the initial rates of MG to DG formation (r_{MG}) also showed a trend consistent with

the selectivity and activity of the investigated materials. The high r_{MG} ratio observed for ACSO3H >HTCSO3H>H-Y and the lowest value observed for homogeneous H_2SO_4 correlated to the shape-selective effects (Table 3.10). In addition, this ratio was also influenced by the dimension of the reacting fatty acid (Table 1.1) and reaction temperature which also supported the shape-selective effects. The increased r_{MG} and reduced initial conversion for oleic acid were in accordance with larger dimensions of reactants and products while decreased values of r_{MG} with temperature suggested that at higher reaction temperature contribution of autocatalytic and surface reaction also increases (Figure 3.12). These results in fact are in agreement with the literature which suggests that in the esterification of fatty acids with glycerol the effects of catalyst on reactivity and selectivity (e.g. for monoglycerides) is at best observed below the autocatalytic temperatures.[30] Irrespective of the catalyst, the selectivity towards monolaurin (desired product) when observed as a function of conversion, typically decreased with increasing conversion due to formation of both DG and TG, as also reported in the previous studies[30,] and also in terms of desired product selectivity, the novel sulfonated catalysts (HTCSO3H and ACSO3H) were the best catalysts. In the current case, the final selectivity to monolaurin at 97 mol-% conversion was 50 mol% while the best monolaurin selectivity was 70% at 92 mol-% conversion over ACSO3H at 125 °C in contrast to the selectivity corresponding to maximum conversion of 81% was 73 mol-% for HTCSO3H (Figure 3.13). In contrast, although monolaurin selectivity was relatively high for the acidic zeolites but the highest conversion levels achieved (45-54 %) were almost half of that achieved for the novel carbon catalysts **[IV]**. Further, the sulfonated catalysts also demonstrated excellent operational stability and only a minor (~14%) activity loss with respect to fatty acid conversion was observed in the 3rd cycle and no changes in selectivity of the desired product were observed **[IV]**. Hence, significant improvements with respect to monolaurin selectivity and process parameters could be achieved when applying sulphonated carbons as a catalyst for esterification of equimolar amounts of fatty acid and glycerol (a temperature reduction of 25 °C) in comparison to a process catalyzed by zeolites, $–SO_3H$ functionalized zeolites or SBA-15 **[IV**].

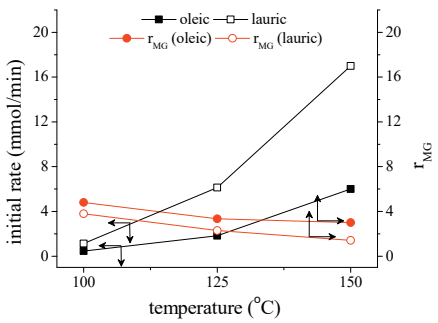

Figure 3.12. Effect of fatty acid and reaction temperature on initial rate of reaction and r_{MG} (the ratio between the initial rates of formation of MG to DG).

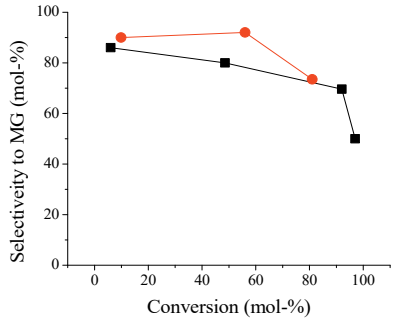

Figure 3.13. Conversion vs. MG selectivity for (■) ACSO3H and (●) HTSO3H at 125 °C.

3.2.6. Cellulose acetylation [V]

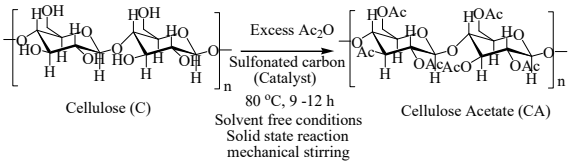

Scheme 3.7. Esterification of cellulose with acetic anhydride to cellulose acetate.

Finally, the catalytic activity of the novel sulfonated carbons (selected: CACS, AC500S, ACSHT and FeCS) were investigated in the solventless acetylation of cellulose with acetic anhydride to cellulose acetate (CA) (Scheme 3.7). The experiment was motivated by the exceptional catalytic activity demonstrated by the novel carbons in glycerol acetylation and cellulose saccharification reactions, which prompted us to further investigate the catalytic potential of these materials in the solid phase reactions. For the sake of comparison, catalytic activities of zeolites (H-Y, H-ZSM-5 and 4-BDS treated H-Y: H-Y-S) and un-modified active carbon (CAC, AC500) were also investigated. Preliminary catalytic tests conducted over the different materials at 80 °C for comparative examination of catalytic activity showed only the strongly Brønsted acidic (with Hammett acidity, H_o comparable to 100% H_2SO_4) i.e. sulfonated carbon materials (CACS, AC500S, ACSHT and FeCS) to be active.[14-16] In contrast, all other materials, zeolites (microporous and H_o comparable to 80% H_2SO_4) and non-sulfonated ACs (H_o comparable to -COOH) were inactive in cellulose acetylation reaction (Table 3.11).[31]

Table 3.11. Overview of the catalytic performance of solid acid catalysts in cellulose acetylation

Catalyst	Reaction time (h)	Ac_2O/AGU (mole ratio)	Catalyst (g)	[a] Yield (%)	DS
Blank	24	9	-	[b]0	-
H-Y	24	9	1	[b]0	-
H-Y-S	24	9	1	[b]0	-
H-ZSM-5	24	9	1	[b]0	-
CAC	24	9	1	[b]0	-
AC500	24	9	1	[b]0	-
CACS	12	9	1	50	2.1
AC500S	12	9	1	77	2.94
AC500S	12	4.5	1	70	2.7
AC500S	12	9	0.5	69	2.67
ACSHT	24	9	1	54	2.3
FeCS	24	9	1	20	1.2

[a] Isolated product yield after separation, washing and vacuum drying at 70 °C, [b]impossible to separate insoluble solid products from catalyst particles (so yield considered to be ~0%).
Reaction conditions: In all experiments the amount of cellulose was 1 g (~6.1 mmol AGU), stirring rate was fixed to 1000 rpm in all the experiments.

Further, among the novel sulfonated materials, the acetylation activities (extent of –OH substitution among acetylated products) were varied directly as a function of material acidity and pore size. In fact, in some cases, the best sulfonated catalyst (AC500S) exhibited catalytic performance which was en par to that of mineral acids (complete acetylation, DS of 2.94 and yield of 77%). To summarize, among the sulfonated materials the activity for cellulose acetylation based on product yield and quality (DS value) was in the order of AC500S >CACS > ACSHT >FeCS; a trend consistent with collective effects of material acidity and porosity (Table 3.2 and 3.3). Overall, these results demonstrated that the sulfonated catalyst with large pores (mesoporosity) and high sulfonic acid site density exhibited high acetylation activity while those with lower acid site density and microporosity were considerably less active (Table 3.11). The optimization experiments performed with the best sulfonated catalyst (AC500S) indicated that, in addition to the catalyst properties, CA yield and quality (DS) were also affected by duration of reaction, the amount of catalyst used and molar ratio of acetic anhydride-to-AGU (CA yield and DS values varied in range of 50-77% and 1.91-2.94, respectively). Here, the optimized condition for producing the commercially desirable CDA (DS 2.7) could be summarized as 80 °C, Ac_2O-to-AGU molar ratio of 4.5 and 12 h reaction time with catalyst to cellulose (w/w) ratio of 1 **[V]**. Visually, success of cellulose acetylation (with the sulfonated materials) could be seen from the steady transformation of the reaction system from an insoluble solid-liquid mixture to highly viscous black liquid which upon dilution with acetone/DMSO and separation of the catalyst particles gave a transparent soluble CA solution (Scheme 3.8). Further, the sulfonated materials (the optimum catalyst, AC500S used as reference) also demonstrated excellent operational stability and were successfully applied during three successive reaction cycles with changes in CA yield and DS. Comparison of our results with the

heterogeneous catalysts reported in earlier studies (SO_4^{2-}/ZrO_2, $H_3PW_{12}O_{40}.6H_2O$ and Amberlyst-15), the sulfonated carbons were not only more active, but also presented several process advantages: the main improvements are (a) the straight-forward recycling and reuse of the catalyst and (b) the possibility to directly convert microcrystalline cellulose under mild, solventless conditions without any prior treatments like ball milling. Further, compared to the traditional solid catalysts, sulfonated carbons are reasonably cheap, easier to synthesize[9] and straight-forward to separate from post reaction mixtures (due to the distinct appearance as a fine black powder, Scheme 3.8).

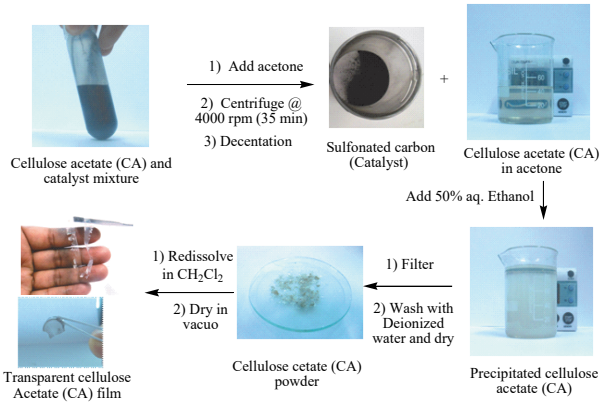

Scheme 3.8. Separation of CA from reaction mixture and preparation of CA film.

Overall, catalytic behavior of sulfonated carbons are analogous to liquid H_2SO_4 and IL [Hmim]HSO_4 and consistent with the role of strong Brønsted acidic $–SO_3H$ groups in cellulose conversion. However, in contrast to the liquid mineral acid catalysts that are offering no control over DS (they produce triacetate exclusively), upon use of sulfonated carbon catalysts it was possible to control the process and selectively to produce CA with different DS values **[V]**. Here, the inability of zeolites to esterify cellulose could also be caused by their limited/narrow pore structures (microporosity) which prevented interaction between the active acid sites and the polymeric cellulose molecules (Table 1.1); while it is most likely that the weakly acidic –COOH and -OH groups of non-sulfonated carbons failed to activate acetic anhydride molecule.[28,29]

The solubility characteristics of the acetylated products (CA) obtained in our study were analogous to those reported by other researchers and consistent with effect of DS value. The ^1H NMR spectrum of a representative CA sample (DS 2.9) illustrating the characteristic $-CH_3$ signals of acetate and cellulose AGU unit -CH at 1.8-2.1 ppm and 3.5-5.0 ppm, respectively, is shown in Figure 3.14. FT-IR patterns of CA also show the characteristic C=O acetate peak at 1750 cm^{-1} and

a correspondingly decreased –OH stretch signal near 3400 cm^{-1} (Figure 3.15).[8,21] The thermal properties of non-derivatized (native) cellulose and soluble cellulose acetate (with a DS value of 2.9) were also characterized by thermogravimetric measurements under N_2 atmosphere (TGA and DTA at heating rate of 10 ◦$Cmin^{-1}$), indicating that the only major weight loss event occurred in the two samples in the temperature range of 300-400 °C. Correspondingly, from the DTA plots the maximum decomposition temperatures of cellulose and cellulose acetate were observed to be at 345 °C and 364 °C, respectively (data not shown). Overall, the TGA and DTA plots indicated that both the onset temperature and the temperature at maximum decomposition rate of CA were higher than those observed for pure cellulose; an observation that is also in accordance with the trends reported in the literature **[V]**.

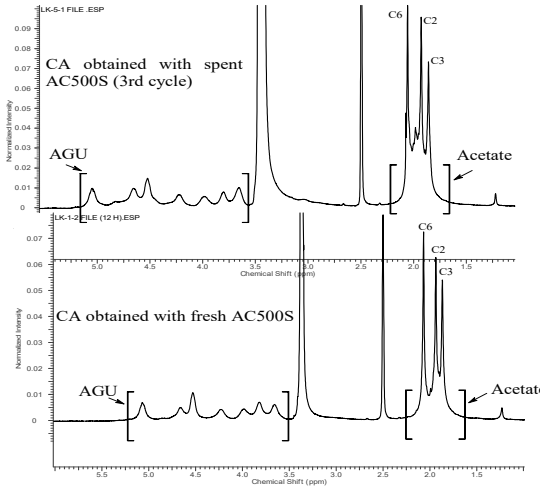

Figure 3.14. ^1H NMR spectra of cellulose acetate (CA) obtained with sulfonated carbon catalyst (AC500S).

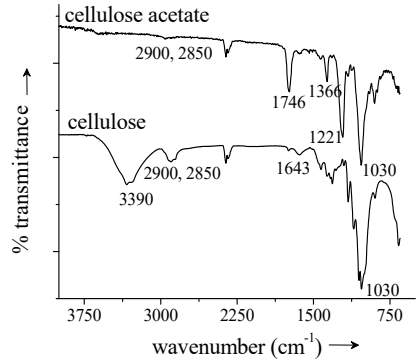

Figure 3.15. FT-IR spectra of cellulose acetate (CA) obtained with sulfonated carbon catalyst (AC500S).

4. Conclusions

Acid-catalyzed saccharification, esterification, transesterification and acetylation are important processes in the valorization chain of biomass (or biomass components) for food, fuel and chemical industries. The agro-industrial waste derived sulfonic acid (–SO_3H/$PhSO_3H$) functionalized novel carbons exhibit excellent catalytic activity in the aforesaid reactions and easily outperformed liquid H_2SO_4 and conventional solid acids (zeolites, ion-exchange resins, etc.). The experimental results revealed strong effects of catalyst pore structure (pore size, porevolume), concentration of –SO_3H groups and surface properties upon activity and selectivity of these catalysts. Here, a large pore catalyst with a high –SO_3H density exhibited the highest esterification and transesterification activity and was successfully employed upon biodiesel production from fatty acids and low grade acidic oils. In addition, the large pore sulfonated catalysts with high total acid density (Jatropha cake based catalysts with high density of –COOH and –OH groups) showed exceptional activity in the saccharification cellulosic materials. The large pore catalysts were also active in selective synthesis of triacetin via glycerol acetylation and out-performed the best zeolite H-Y. They also demonstrated equally good activity in acetylation of cellulose to soluble cellulose acetates, with the possibility to control cellulose acetate yield and quality (DS) by a simple adjustment of reaction duration and acetic anhydride amount. On the other hand, the small pore and highly functionalized catalysts obtained by the hydrothermal method and from protein-rich Jatropha DOWC were active in the selective esterification of glycerol to monolaurin and cellulose saccharification, respectively. The operational stability and reusability of the catalyst was found to be dependent on the stability of the SO_3H function (leaching) as well as on the active site blocking due to adsorption of impurities during the reaction. The catalyst decay model proposed upon biodiesel production showed that the catalyst lost its activity mainly due to active site blocking by adsorption of impurities. The potential of DOWC derived sulfated mesoporous active carbons as efficient integrated solid acid catalysts for valorization of biomass to platform chemicals, biofuel, bio-additive, surfactants and cellulose-esters was clearly demonstrated. Therefore, considering all aspects of the catalysts developed (activity, stability and reusability), the continuous flow stirred-tank reactor (CSTR) may be recommended for applications in liquid phase reactions. Nonetheless, additional studies with more reactor systems/types are needed to recommend the optimal reactor systems and operation conditions.

Notations

4-BDS	4-benzenediazoniumsulfonate
BET	Brunauer–Emmett– Teller
BJH	Barrett-Joyner-Halenda
$CDCl_3$	Chloroform-d
DOWC	De-oiled waste cake
DTBG	di-tert-butyl-glycerol
EDX	Energy-dispersive X-ray spectroscopy
FAAE	Fatty acid alkyl ester
FAME	Fatty acid methyl ester
FFA	Free Fatty Acids
FT-IR	Fourier transform infrared spectroscopy
GTBE	glycerol-tertiary-butyl-ether
GHG	Green house gas
GC	Gas chromatography
GC-MS	Gas chromatography mass spectrometry
H_	Hammett strength
HPLC	High precision liquid chromatography
IEA	International energy agency
k	Rate constant
NMR	Nuclear magnetic resonance spectroscopy
$PhSO_3H$	Phenyl sulfonic acid
SEM	Scanning electron microscopy
$-SO_3H$	Sulfonic acid
TIC	Total ion chromatogram
TEM	Transmission electron microscopy
T	Time
T	Temperature
$T_{(max)}$	Thermal stability
TBA	tert-butyl alcohol
TGA	Thermogravimetric analysis
TMS	Tetramethylsilane
TOF	Turnover frequency
TPD	Temperature programmed desorption
XRD	X-ray Diffraction
XPS	X-ray photoelectron spectroscopy

References

1. P. C. A. Bruijnincx, Y. Román-Leshkov, Sustainable catalytic conversions of renewable substrates, Catal. Sci. Technol., 2014, **4**, 2180.
2. M. Besson, P. Gallezot, C. Pinel, Conversion of biomass into chemicals over metal catalysts, Chem. Rev. 2014, **114**, 1827−1870.
3. Technology Roadmaps Biofuels for transport, IEA, 2011.
4. P. Fairley, Introduction: Next generation biofuels, Nature, 2011, **474**, S2–S5.
5. D. M. Alonso, J. Q. Bond, J. A. Dumesic, Catalytic conversion of biomass to biofuels, Green Chem., 2010, **12**, 1493–1513.
6. M. J. Climent, A. Corma, S. Iborra, Conversion of biomass platform molecules into fuel additives and liquid hydrocarbon fuels, Green Chem., 2014, **16**, 516-547.
7. O. D. Mante, J. A. Rodriguez, S. D. Senanayake, S. P. Babu, Catalytic conversion of biomass pyrolysis vapors into hydrocarbon fuel precursors, Green Chem., 2015, **17**, 2362-2368.
8. M. Pagliaro, R. Ciriminna, H. Kimura, M. Rossi M, C. Della Pina, From Glycerol to Value-Added Products, Angew. Chem. Int. Ed. 2007, **46,** 4434 – 4440.
9. S. Fischer, K. Thu¨mmler, B. Volkert, K. Hettrich, I. Schmidt, K. Fischer, Macromolecular Symposia, 2008, **262**, 89–96.
10. J. Jae, G. A. Tompsett, A. J. Foster, K. D. Hammond, S. M. Auerbach, R. F. Lobo, G. W. Huber, Investigation into the shape selectivity of zeolite catalysts for biomass conversion, J. Catal., 2011, **279**, 257–268.
11. <http://www.iza-online.org> (cited 13.05.2015).
12. C. Magne, M. Urien, I. Ciofini, T. Tugsuz, T. Pauporte, Amphiphilic acids as co-adsorbents of metal-free organic dyes for the efficient sensitization of nanostructured photoelectrode, RSC Advances, 2012, **2**, 11836–11842.
13. J.A. Janaun, Development of sulfonated carbon catalysts for integrated biodiesel production, (PhD Thesis) The University of British Columbia (Vancouver), 2012.
14. L.J. Konwar, J. Boro, D. Deka, Review on latest developments in biodiesel production using carbon-based catalysts, Renew Sust Energ Rev, 2014, **29**, 546–564.
15. (a) K. Nakajima, M. Hara, Amorphous carbon with SO_3H groups as a solid Brønsted acid catalyst, ACS Catal.. 2012, **2(7)**, 1296–1304; (b) M. Hara, T. Yoshida, A. Takagaki, T. Takata, J.N. Kondo, S. Hayashi, K. Domen, A carbon material as a strong protonic acid,

Angewandte Chemie-International Edition. 2004, **43**, 2955–8; (c) M. Toda, A. Takagaki M. Okamura, J.N. Kondo, S. Hayashi, K. Domen, Green chemistry – biodiesel made with sugar catalyst. Nature 2005, **438**, 178.

16. (a) M. Hara, Biomass conversion by a solid acid catalyst, Energy Environ Sci. 2010, **3**, 601–607; (b) X. Mo, D.E. López, K. Suwannakarn, Y. Liu, E. Lotero, J.G. Goodwin Jr, Activation and deactivation characteristics of sulfonated carbon catalysts, J. Catal., 2008, **254,** 332–338.

17. M. Keiluweit, P. S. Nico, M. G. Johnson, M. Kleber, Dynamic molecular structure of plant biomass-derived black carbon (biochar), Environ. Sci. Technol., 2010, **44(4)**, 1247–1253.

18. P.J.F. Harris, Z. Liu, K. Suenaga, Imaging the atomic structure of activated carbon. J. Phys.: Condens. Matter, 2008, **20**, 362201-362205.

19. L.J. Konwar, R. Das, A.J. Thakur, E. Salminen, P. Mäki-Arvela, N. Kumar, J.P. Mikkola, D. Deka, Biodiesel production from acid oils using sulfonated carbon catalyst derived from oil-cake waste, J. Mol. Cat. A, 2014, **388–389**, 167-176.

20. M. Käldström, N. Kumar, T. Heikkilä, M. Tiitta, T. Salmi, D. Yu. Murzin, Formation of Furfural in Catalytic Transformation of Levoglucosan over Mesoporous Materials, ChemCatChem, 2010, **2**(5), 539–546.

21. A. Onda, T. Ochi, K. Yanagisawa, Hydrolysis of cellulose selectively into glucose over sulfonated activated-carbon catalyst under hydrothermal conditions, Top. Catal., 2009, **52**, 801–807.

22. T.C. Nagaiah, A. Bordoloi, M.D. Sanchez, M. Muhler, W. Schuhmann, Mesoporous nitrogen-rich carbon materials as catalysts for the oxygen reduction reaction in alkaline solution, ChemSusChem, 2012, **5**, 637–641.

23. J.R. Kastner, J. Millera, D.P. Geller, J. Locklin, L.H. Keith, T. Johnson, Catalytic esterification of fatty acids using solid acid catalysts generated from biochar and activated carbon, Catal. Today, 2012, **190**, 122–132.

24. J.T. Yu, A.M. Dehkhoda, N. Ellis, Development of biochar-based catalyst for transesterification of canola oil, Energy Fuels, 2010, **25**, 337–344.

25. R.A. Arancon, H.R. Barros Jr., A.M. Balu, C. Vargas, R. Luque, Valorisation of corncob residues to functionalised porous carbonaceous materials for the simultaneous esterification/transesterification of waste oils, Green Chem. 2011, **13**, 3162–3167.

26. P. Mäki-Arvela, I. Anugwom, P. Virtanen, R. Sjöholm, J.P. Mikkola, Dissolution of lignocellulosic materials and its constituents using ionic liquids—a review, Ind. Crops Prod., 2010, **32**, 175–201.

27. J. Pang, A. Wang, M. Zhenga, T. Zhang, Hydrolysis of cellulose into glucose over carbons sulfonated at elevated temperatures, Chem. Commun., 2010, **46**, 6935–6937.

28. T.H. Lowry, K.S. Richardson, Mechanism and Theory in Organic Chemistry, Scsecond ed., Harper & Row, New York, 1981. 652–658.

29. L.N. Silva, V.L.C. Gonçalves, C.J.A. Mota, Acetylation of glycerol with acetic anhydride, Catal. Commun., 2010, **11**, 1036–1039.

30. E. Heykants, W. H. Verrelst, R. F. Parton, P. A. Jacobs, Shape-selective Zeolite catalysed synthesis of monoglycerides by esterification of fatty acids with glycerol, Studies in Surface Science and Catalysis, 1997, **105**, 1277–1284.

31. P.A. Wright. Microporous Solid Acid Catalysts and their Applications, In Microporous Framework Solids, RSC publications, 2007, 312-371.

32. E.M. Kondili, J.K. Kaldellis**,** Biofuel implementation in East Europe: Current status and future prospects**,** Renew Sust Energ Rev**,** 2007, **11**(9), 2137-2151.

Original Publications

[I]. **Lakhya Jyoti Konwar,** Päivi Mäki-Arvela, Eero Salminen, Narendra Kumar, Ashim Jyoti Thakur, Jyri-Pekka Mikkola, Dhanapati Deka. Towards carbon efficient biorefining: Multifunctional mesoporous solid acids obtained from biodiesel production wastes for biomass conversion. Appl.Cat. B Env., 176–177, 20–35, 2015.

[II]. **Lakhya Jyoti Konwar**, Johan Wärnå, Päivi Mäki-Arvela, Narendra Kumar, Jyri-Pekka Mikkola. Reaction kinetics with catalyst deactivation in simultaneous esterification and transesterification of acid oils to biodiesel (FAME) over a mesoporous sulphonated carbon catalyst, Fuel, 166, 1-11, 2016**.**

[III]. **Lakhya Jyoti Konwar,** Päivi Mäki-Arvela, Pakiza Begum, Narendra Kumar, Ashim Jyoti Thakur, Jyri-Pekka Mikkola, Ramesh Chandra Deka, Dhanapati Deka. Shape selectivity and acidity effects in glycerol acetylation with acetic anhydride: Selective synthesis of triacetin over Y-Zeolite and sulfonated mesoporous carbons, J. Catal., 329, 237-247, 2015.

[IV]. **Lakhya Jyoti Konwar**, Päivi Mäki-Arvela, Narendra Kumar, Jyri-Pekka Mikkola, Anil Kumar Sarma, Dhanapati Deka. Selective esterification of fatty acids with glycerol to monoglycerides over $–SO_3H$ functionalized carbon catalysts, React.Kin.Mech.Cat. 2016 (accepted, in press)

[V]. **Lakhya Jyoti Konwar**, Päivi Mäki-Arvela, Ashim Jyoti Thakur, Narendra Kumar, Jyri-Pekka Mikkola. Sulfonated carbon as a new, reusable heterogeneous catalyst for one-pot synthesis of acetone soluble cellulose acetate, RSC Advances, 6, 8829-8837, 2016.

[VI]. **Lakhya Jyoti Konwar**, Yasuhito Sugano, Rahul Singh Chutia, Päivi Mäki-Arvela, Rupam Kataki, Jyri-Pekka Mikkola. Sustainable synthesis of N and P co-doped porous amorphous carbon using oil seed processing wastes, Materials Letters, 173, 145–148, 2016.

ISBN 978-952-12-3395-1 (print)
ISBN 978-952-12-3396-8 (PDF)
Painosalama Oy – Turku, Finland 2016